applied sciences

MDPI

Article

Biosynthesis of Silver Nanoparticles Using *Barleria albostellata* C.B. Clarke Leaves and Stems: Antibacterial and Cytotoxic Activity

Serisha Gangaram [1,*], Yougasphree Naidoo [1], Yaser Hassan Dewir [2], Moganavelli Singh [1], Johnson Lin [1], Aliscia Nicole Daniels [1] and Nóra Mendler-Drienyovszki [3]

[1] School of Life Sciences, University of KwaZulu-Natal, Westville Campus, Private Bag X54001, Durban 4000, South Africa; naidooy1@ukzn.ac.za (Y.N.); singhm1@ukzn.ac.za (M.S.); linj@ukzn.ac.za (J.L.); alisciadaniels@gmail.com (A.N.D.)

[2] Plant Production Department, College of Food and Agriculture Sciences, King Saud University, Riyadh 11451, Saudi Arabia; ydewir@ksu.edu.sa

[3] Research Institute of Nyíregyháza, Institutes for Agricultural Research and Educational Farm (IAREF), University of Debrecen, P.O. Box 12, 4400 Nyíregyháza, Hungary; mendlerne@agr.unideb.hu

* Correspondence: serishagangaram@yahoo.com

Abstract: Silver nanoparticles (AgNPs) have increasingly gained attention owing to their distinctive physicochemical and biological properties. The objective of the investigation was to biologically synthesize AgNPs using plant extracts from *Barleria albostellata*. The synthesized AgNPs, obtained from *B. albostellata* (leaves and stems), were characterized through various techniques including UV-visible spectroscopy, scanning electron microscopy (SEM), high-resolution transmission electron microscopy (HRTEM), energy-dispersive X-ray analysis, Fourier transform infrared (FTIR) spectral analysis, and nanoparticle tracking analysis (NTA). The antibacterial efficacy of the synthesized AgNPs was evaluated utilizing the disk diffusion method. The cytotoxicity effects of the synthesized AgNPs were determined using the MTT assay (3-[(4,5-dimethylthiazol-2-yl)-2,5-diphenyl tetrazolium bromide]) in cervical cancer (HeLa), embryonic kidney (HEK293), and breast adenocarcinoma (MCF-7) cell lines. The results indicate that *B. albostellata* extracts could serve as eco-friendly biofactories for the synthesis of AgNPs. UV-vis spectroscopy of the leaf and stem extracts revealed absorption peaks within the range of 400–450 nm, thereby confirming the synthesis of AgNPs. Elemental Ag was highest in the methanol leaf extracts (16.87 ± 0.89%) and lowest in the powdered stem extracts (7.13 ± 1.44%). Synthesized AgNPs were predominantly spherical in shape. HRTEM revealed that synthesized AgNPs from the methanolic stem extracts (34.32 ± 16.99 nm) were larger in size, while those from the powdered stem extracts were smaller (16.57 ± 5.55 nm). AgNPs synthesized from both the leaf and stem extracts exhibited zeta potential values between −8.8 and −32.1 mV, with hydrodynamics diameters ranging from 34.3 to 111.3 nm. FTIR spectroscopy confirmed the presence of various functional groups on the AgNPs. AgNPs synthesized from the leaf and stem extracts displayed significant antibacterial activity and were sensitive to Gram-negative and Gram-positive bacteria. AgNPs exhibited significant antibacterial activity (diameter of the zone of inhibition) against *Pseudomonas aeruginosa* (21.67 ± 2.87 mm) in the leaf methanolic extract. Synthesized AgNPs exhibited selective in vitro cytotoxicity against HEK293, HeLa, and MCF-7 cell lines. The IC_{50} values of the AgNPs synthesized from the various extracts were all above 9 µg/mL. Significant cytotoxic levels (IC50 16.11 and 27.23 µg/mL) were observed for the MCF-7 cell line upon exposure to the methanolic leaf and stem AgNPs. This study recommends the use of medicinal plant extracts in producing economically effective AgNPs, due to their efficient capping. Overall, AgNPs synthesized from *B. albostellata* extracts comprised novel antibacterial and anticancer agents, and warrant further investigation. Bio-synthesized AgNPs show great potential in the area of nanotechnology and may be used as an affordable, eco-friendly alternative for the delivery of conventional therapeutics.

Keywords: antibacterial activity; biofactories; biosynthesis; cytotoxicity; elemental Ag^+

Citation: Gangaram, S.; Naidoo, Y.; Dewir, Y.H.; Singh, M.; Lin, J.; Nicole Daniels, A.; Mendler-Drienyovszki, N. Biosynthesis of Silver Nanoparticles Using *Barleria albostellata* C.B. Clarke Leaves and Stems: Antibacterial and Cytotoxic Activity. *Appl. Sci.* **2024**, *14*, 8331. https://doi.org/10.3390/app14188331

Academic Editor: Gang Wei

Received: 30 July 2024
Revised: 1 September 2024
Accepted: 11 September 2024
Published: 16 September 2024

1. Introduction

Nanotechnology is an emerging research discipline focusing on the synthesis and application of small particles called nanoparticles (NPs) (<100 nm) [1–3]. The term "Nano" originates from Latin, meaning dwarf. The advancement of molecular technology has facilitated the manipulation of atoms and molecules of certain materials, such as plants, resulting in the reduction to nanoparticles ranging from 1–100 nm in size [4,5]. This field has various applications in biology, chemistry, energy science, medical science, and pharmaceutics [6–8]. The use of natural reagents as reductants and capping agents, such as biodegradable polymers, sugars, microorganisms, and plant extracts, are desirable for nanotechnology [9]. Nanomedicine links the gap between the physics of nanostructures and the biology leading to their medicinal importance [10]. Green syntheses, the eco-friendly processes utilized in the field of chemistry, are increasingly gaining popularity due to their potential in addressing global environmental issues [9,11]. To achieve this objective, the utilization of natural resources (organic systems) and model solvent systems is imperative [12]. While the microbial approach to synthesize NPs is considered environmentally friendly, the utilization of plant materials in their production may be more advantageous, given the intricate steps involved in surface modification and the time-consuming nature of microbial screening [9,13]. Biosynthetic methods use plant extracts to act as reducing and capping agents [14–16] and have emerged as a straightforward, viable, and environmentally friendly substitute for the more intricate chemical synthesis procedures for nanomaterials [17,18]. Although the precise mechanism of synthesizing NPs using plant extracts remains unclear, it has been observed that biomolecules such as alkaloids, phenols, and flavonoids present in these extracts play a crucial role in reducing metal ions and capping the biosynthesized NPs [19,20]. There has been great interest in metal NPs such as gold (Au) [21], copper (Cu) [22], and silver (Ag) [23–25] for treating various ailments due to their unique characteristics in terms of size, shape, and biological properties [26].

Cancer stands as a predominant cause of mortality in Africa, with 70% of deaths occurring in low to middle income countries [27]. Despite this, the focus on infectious diseases has taken precedence over cancer in the public health agenda of several African countries [28]. The administration of chemotherapy drugs for cancer treatment poses challenges due to their non-specific nature, leading to the development of multidrug resistance and subsequent toxicities associated with chemotherapy. As a result, patients often succumb to the adverse effects of the drugs rather than the disease itself [29,30]. Antimicrobial resistance in South Africa is estimated to be linked with over 700,000 deaths every year. In 2018, cancer and benign tumors accounted for 9.7% of all mortality in the country [27,28]. Nanomaterials are poised to revolutionize cancer treatment by enhancing early detection, prognosis, and therapy. NPs are expected to provide targeted delivery, enhanced efficacy of therapeutic agents, and resistance to multidrug resistance mechanisms [31,32]. Additionally, NPs play a crucial role as antibacterial agents, especially in light of the rapid evolution of disease-causing microorganisms and their increasing resistance to traditional biocides [23,24]. This necessitates the urgent development or modification of alternative treatments and antimicrobial compounds [2,33]. Among all the metal NPs, silver NPs (AgNPs) have gained substantial attention due to their availability [34,35] and their diverse applications in therapeutics, including antimicrobial, antidiabetic, anticancer, and antioxidant activities [36,37]. AgNPs are the most commercialized nanomaterial globally, with an annual production of five hundred tons [38,39]. The application of AgNPs in various fields, such as artificial implants, diagnostics, tissue engineering, imaging, sensing, and gene and drug delivery, is linked to their unique optical, electrical, and thermal characteristics [40,41]. Several medicinal phytochemicals have been documented to reduce, cap, and stabilize Ag^+ ions [42,43]. Several reducing agents, specifically Tollens reagent, ascorbate, elemental hydrogen sodium citrate, and polyol sodium borohydride, reduce silver ions (Ag^+) in non-aqueous or aqueous extracts [44]. There are three reactant elements that are necessary for the standard preparation of AgNPs, and these include a metal precursor, reducing agents, and stabilizing agents [45]. Plant-mediated biosynthetic methods are widely used

for the rapid production of AgNPs with polar solvents (methanol and water) being reported to be highly effective in their synthesis [46]. The morphological limitations of synthesizing NPs (e.g., shape and size) can be controlled by changing the reaction conditions and concentrations of chemicals (e.g., pH and temperature) [12].

Barleria albostellata (Acanthaceae), an indigenous shrub found in the tropical and subtropical regions of South Africa [47], is recognized for its medicinal attributes, particularly the antibacterial and anti-inflammatory properties exhibited by its leaf and stem extracts [48]. Despite a lack of scientific data on the traditional medicinal use of *B. albostellata*, other species within the genus have been historically employed for their diverse pharmacological activities [48–55]. Gangaram et al. [56] have found the leaves and stems of *B. albostellata* to be rich in bioactive compounds and a possible source of antibacterial agents. Additionally, the leaves and stems exhibited strong antioxidant activity correlating to its cytotoxicity [57]. Plant metabolite profiles can differ among various plant parts [58,59]. The current study aimed to synthesize and characterize the methanolic and aqueous AgNPs using various protocols, evaluate their antibacterial activity against Gram-positive and Gram-negative bacteria using the disk diffusion method, and assess their cytotoxicity activity using the 3-(4,5-dimethylthiazol-2-yl)-2,5-diphenyl-2H-tetrazolium bromide (MTT) assay against several cancer cell lines. To our knowledge, there are no previous reports on the biosynthesis of NPs from extracts of *B. albostellata*. Thus, investigation on the synthesis of AgNPs using *B. albostellata* is essential to elucidate its potential use in the nanotechnology industry.

2. Materials and Methods

2.1. Plant Materials

Leaves and stems from *B. albostellata* were collected from the University of KwaZulu–Natal (UKZN), Westville campus (29°49′51.6″ S, 30°55′30″ E), situated in Durban, South Africa. A voucher specimen (7973000) was deposited in the Ward Herbarium, UKZN.

2.1.1. Preparation of the Methanolic Crude Extract

The leaf and stem materials were oven-dried for 2 weeks at 35 °C. The oven-dried materials were crushed into a fine powder using a blender (Russel Hobbs, model: RHB315, Durban, South Africa) and then extracted using methanol in a Soxhlet apparatus. Approximately 10 g of powdered leaves were placed into a round-bottom flask containing 100 mL of methanol, which was subsequently boiled at 40 °C for three hours. The extract was filtered using Whatman® No. 1 filter paper and stored for further experimentation. This process was repeated three times. Sequential extractions were performed on both leaf and stem materials. The resultant extracts were transferred into glass containers and maintained at 4 °C until they were used for subsequent analyses.

2.1.2. Fresh Aqueous Extract

The fresh plant material was extracted according to Govindarajan and Benelli [60], with modifications. Approximately 35 g of washed and cut leaf and stem materials were added into 600 mL beakers. Sterile distilled water (100 mL) was added to each beaker and placed in an oven for 30 min at 60 °C. Extracts were filtered, transferred into glass jars, and then stored at 4 °C until further use.

2.1.3. Powdered Aqueous Extract

Approximately 10 g of powdered leaf and stem materials were added into a 250 mL Erlenmeyer flask, followed by the addition of 100 mL of sterile distilled water. Solutions were mixed and heated in an oven at 60 °C for 3 h. Thereafter, the samples were filtered and transferred to glass jars and stored at 4 °C until further use.

2.1.4. Synthesis of AgNPs

The silver nitrate ($AgNO_3$, 1 mM) (Merck, Durban, South Africa) aqueous solution was made using deionized water. The reduction of Ag^+ ions was facilitated by the incorporation of 10 milliliters of extract (comprising both leaves and stems) into 90 mL of the $AgNO_3$ solution [61,62]. A pH level of 7 was determined to be optimal to ensure Ag^+ was reduced to metallic silver (Ag^0). The solution was incubated at 80 °C for a period of 3 h, until a colour change was observed. The formation of AgNPs was indicated by the emergence of a brownish colour [63]. Upon intensification of the solution's color, the conical flasks were removed to prevent the agglomeration of AgNPs, which typically occurs when the solution exhibits a dark coloration [64]. All analyses were performed in triplicate.

2.1.5. Quantification of AgNPs

Subsequent to the synthesis, the reaction mixture (comprising methanolic, fresh, and powdered aqueous extracts) of leaf and stem was dispensed into centrifugal tubes. Each solution was augmented with 20 mL of distilled water and centrifuged (BECKMAN COULTER, Avanti® J-E Centrifuge, Brea, CA, USA) at 4 °C for 20 min at 10,000 rpm, thereby yielding a concentrated pellet. The supernatant from each solution was discarded, and the pellet was replenished with deionized water. Centrifugation was repeated thrice to eliminate unreacted materials, which may exist as either compounds or biomass residues, including any free enzyme or protein molecules not bound to the AgNPs. The pellet was subsequently dispersed in deionized water and vortexed for 5 min (Vortex Mixer Model VM-1000, Cole-Parmer, Johannesburg, South Africa). The resulting suspension of each extract was oven-dried at 50 °C for 7 days. The yield of the synthesized AgNPs from each extract was quantified utilizing the following equation and subsequently characterized as the following:

$$\text{Extract yield } (\%) = \text{Weight of dried extract } (g)/\text{weight of plant material } (g) \times 100$$

2.1.6. Characterisation of AgNPs

UV-visible spectroscopy

AgNP synthesis was determined by examining each colloidal solution (1 mL) after synthesis using the SHIMADZU UV-1800 Spectrophotometer (Cole-Parmer, Duisburg, Germany) at a range of 200–800 nm at a medium speed, using 1 mM $AgNO_3$ solution as a blank. The absorption spectra for each sample were correlated to that found in the literature, confirming their successful synthesis. Prior to analysis, all synthesized samples were sonicated (SONICLEAN, Austrailia sonication bath) and vortexed for 5 min in order to ensure uniformity of the solution.

Ultra Plus field emission gun Scanning electron microscopy (SEM)

Approximately 2 mL of each synthesized NP solution was pipetted separately into 3 mL Eppendorf Tubes® and sonicated (SONICLEAN, sonication bath) for 20 min. Thereafter, approximately 20 µL of each solution was pipetted onto aluminium stubs and left to dry for 60 min beneath a mercury lamp. The stubs were sputter coated with gold using the Quorum 150 RES. Samples were viewed and analyzed on an Ultra Plus field emission gun scanning electron microscope (FEGSEM) (Carl Zeiss, Jena Germany). Images were captured using the SmartSEM imaging software 8.0.

Energy-dispersive X-ray spectroscopy (EDX)

Energy dispersive X-ray spectroscopy analytically detects elemental compositions present in any material. The synthesized NP solutions of the leaves and stems were sonicated (SONICLEAN, sonication bath) for 20 min. Thereafter, approximately 20 µL of each solution was dispensed onto a glass coverslip attached to an aluminium stub containing double-sided adhesive carbon tape. Solutions were dried under a mercury lamp for about 60 min. The elemental composition of the NPs produced from the leaf and stem

methanolic extracts were identified using the Aztec analysis software 1.2 on the Ultra Plus FEGSEM (Carl Zeiss, Germany) at 5 kV.

High-resolution transmission electron microscopy (HRTEM)

The shape, size, and distribution of the synthesized AgNPs produced from leaves and stems were analysed with the HRTEM. Each solution was sonicated (SONICLEAN, sonication bath) to ensure that the AgNPs were evenly distributed. Formvar carbon coated grids (400-mesh) (Ted Pella Inc., Redding, CA, USA) were dipped in each solution and placed under a lamp for 1 h at room temperature to allow the solvent to evaporate. Samples were viewed under the JEOL JEM HRTEM 2100 (Tokyo, Japan) at 200 kV. ImageJ software Java 1.53e was used to determine the size of the AgNPs.

Nanoparticle Tracking Analysis (NTA)

To precisely elucidate the zeta potential, size distribution, and nano-complexes of all synthesized AgNPs, NTA (Nanosight NS-500, Malvern Instruments, UK) was conducted at a temperature of 25 °C. Approximately 2 mL of each nanoparticle solution (methanolic, aqueous-fresh, and aqueous-powdered AgNPs) was extracted and transferred into Eppendorf tubes (3 mL). A dilution of 1 mL at a ratio of 1:500 (in 18 Mohm water/Ultrapure Millipore water) of each extract was prepared in suspension for analysis, aimed at determining the hydrodynamic diameter. All samples underwent triplicate analyses. Images were viewed, captured, and evaluated using the NTA 3.2 analytical software.

Fourier transform infrared spectroscopy (FTIR)

In order confirm the presence of capping functional groups in the AgNPs, infrared spectroscopy of the dried leaf and stem extracts and their synthesized AgNPs was achieved using the Agilent Cary 630 spectrometer using Agilent MicroLab PC 5.1.22. Resolution Pro 5.0.0.395 was used to process the data for peaks. The data were collected using ATR Diamond^{-1} Bounce with 30 background scans and 30 sampling scans with a resolution of 4 cm^{-1}. The detection of peaks displayed by the various function groups were scanned at a range between 3800–800 cm^{-1}.

2.1.7. Antibacterial Bioassays

Test microorganisms

The antibacterial efficacy of both leaf and stem AgNP samples was evaluated against five distinct strains of bacteria. These strains included Gram-positive bacteria: *Bacillus subtilis* (ATCC 6633), methicillin-resistant *Staphylococcus aureus* (ATCC 43300), and *Staphylococcus aureus* (ATCC 25923), in addition to Gram-negative bacteria: *Pseudomonas aeruginosa* (ATCC 25783), and *Escherichia coli* (ATCC 35218). The aforementioned bacterial strains were provided by Professor Johnson Lin from the School of Life Sciences (Microbiology Department) at UKZN, and were preserved in a 75% glycerol solution at −80 °C for experimental use.

Preparation of sample

Synthesized nanoparticles were obtained from methanolic, aqueous-fresh, and powdered leaf and stem extracts. These extracts were further dissolved in a 10% dimethyl sulfoxide (DMSO) solution at different concentrations of 100, 50, 25, 12.5, 6.25, and 3.125 mg/mL. Samples were then transferred into Eppendorf tubes (mL) and stored at 4 °C in preparation for further experimental procedures.

Preparation of culture media and bacterial cultures

Mueller–Hinton agar (MHA, 38 g) (Biolab, Merck, South Africa) was dissolved in 1 L of distilled water, agitated for 15 min, microwave heated for 10 min, and then autoclaved (Model HL-340, Durban, South Africa) for a duration of 1 h at 121 °C. The medium was aliquoted into Petri dishes (sterile) (90 mm) and cooled at room temperature (23 °C). Each bacterial strain, encompassing both Gram-positive and Gram-negative categories, was

sub-cultured onto freshly prepared agar plates and incubated overnight (24 h) at 37 °C. Glass test tubes containing 15–20 mL of distilled water were similarly autoclaved at 121 °C for 1 h. Bacterial colonies from each agar plate were inoculated by transferring 5 $\mu g \cdot \mu L^{-1}$ of the respective strain into the prepared glass test tubes containing 15 mL of sterile distilled water, corresponding to the 0.5 McFarland scale. The absorbance of each bacterial culture was subsequently measured, adjusted, and diluted to achieve an appropriate viable cell count utilizing a Cary 60 UV-Vis spectrophotometer (Agilent Technologies, Santa Clara, CA, USA).

Freshly cultured bacterial strains were uniformly distributed over the MHA plates using an L-shaped metal spreader (hockey stick). The disk diffusion method was employed to evaluate the antibacterial properties of the synthesized AgNPs. Approximately 20 µL of AgNPs, prepared using the methanolic and aqueous-fresh and powdered extracts, were carefully pipetted onto sterile filter paper discs (Whatman® no. 1 filter paper) with a diameter of 6 mm. Sterile discs impregnated with AgNPs at various concentrations were allowed to dry overnight before being positioned onto Petri plates inoculated with bacterial cultures. The Petri plates were subsequently sealed and incubated for 24 h at 37 °C. The presence of clear zones of inhibition surrounding the filter paper was recorded as indicative of positive antibacterial results, and the diameters of these zones were measured and documented within 18–24 h post-incubation to ascertain whether the synthesized AgNPs exhibited antibacterial activity. The clear zones of inhibition were quantified and tabulated. Filter paper discs containing streptomycin and gentamycin served as positive controls, while 10% DMSO was utilized as a negative control. The analyses were conducted in triplicate, and the data were presented as mean ± standard deviation.

2.1.8. In Vitro Cytotoxicity/MTT Assays

Cell cultures

The cytotoxic effects of the AgNPs were assessed in cervical carcinoma cells (HeLa), human embryonic kidney (HEK293) cells, and breast adenocarcinoma (MCF-7) cells. Cell lines (Cryopreserved) were obtained from the American Type Culture Collection (ATCC) situated in Manassas, VA, USA. The experimental procedures involving cell cultures were conducted within a sterile class II biohazard safety cabinet. Cryopreserved cell lines, which were maintained at −80 °C in a Nuaire biofreezer, were retrieved and then defrosted at 37 °C in a water bath. Aseptically, the cell suspensions were placed into falcon centrifuge tubes and centrifuged (Eppendorf benchtop centrifuge) for 5 min at 1000 rpm, after which the supernatant was discarded. The resulting pellet was then re-suspended in 1 mL of whole sterile medium (Eagle's Minimum Essential Medium (EMEM)) augmented with 1% antibiotics (100 µg/mL streptomycin, 100 units/mL penicillin,) and 10% Foetal Bovine Serum (FBS). The cell suspensions were subsequently dispensed and cultured in a 25 cm^2 tissue culture flask which contained 4 mL of whole sterile medium. These cells were then incubated at 37 °C (Thermo-Electron Corporation, Waltham, MA, USA) in an atmosphere containing 5% CO_2 and observed daily using an inverted microscope (Nikon TMS-F 6V, Tokyo, Japan). The sterile whole medium was routinely replaced until the cells reached confluency [65].

MTT (cell viability) assay protocol

The assay employed aimed to quantify the metabolic activity of cells and their ability to reduce MTT into formazan using the succinate-tetrazolium reductase system [66]. The cells were subjected to trypsinization and subsequently seeded into 96-well microtiter plates, where they were incubated overnight at 37 °C to allow for cell attachment. Thereafter, the medium was substituted with new medium (EMEM + 10% FBS + 1% Antibiotics) [65]. Cells were then treated with different concentrations of synthesized AgNPs from *B. albostellata* (15, 30, 60, 120, and 140 µg/mL) and incubated for 48 h at 37 °C. In each well, the growth medium was aspirated and 100 µL of medium (comprising 10 µL of the MTT solution (5 mg/mL in phosphate buffered saline (PBS) solution) was added, followed by a 4 h

incubation at 37 °C. Subsequently, the medium containing MTT was removed from each well and replaced with 100 µL of DMSO to ensure a complete solubilization of the formazan crystals. The formation of these crystals served as an indicator of cellular viability [67]. Once DMSO was added, the solution exhibited a purple coloration. The absorbance of the solution was measured at 570 nm using the Mindray M-R-96A microplate reader (Vacutec, Hamburg, Germany) and DMSO as the control. Solutions which contained cells only served as the positive controls and was recorded as 100% survival [65]. This protocol was conducted in triplicate. Graphs were created using Microsoft Excel 2019™ in order to determine the concentration at which 50% cell death was attained (IC50).

2.1.9. Statistical Analysis

All analyses were completed in triplicate. Values obtained were displayed as mean ± standard deviation. These values were then subjected to statistical analysis using the R statistical computing software, 2020, version 3.6.3. Data obtained were subjected to One-Way Analysis of Variance (ANOVA) followed by Tukey's honest significant difference multiple range post hoc tests. Data were expressed as mean significant at the $p < 0.05$ level.

3. Results and Discussion

3.1. Synthesis of AgNPs and UV Characterisation

The reduction of $AgNO_3$ in leaf and stem extracts after 3 h of incubation at 80 °C was visually evident by color changes (brownish-yellow) in the reaction mixture (Figure 1). These changes in color indicate the production of AgNPs [7,59] due to the reduction of Ag^+ to Ag^0 by numerous biomolecules that are present in the plant extract [60]. Our results showed that the brown color intensity increased with the duration of the incubation period. However, after 3 h, there were no visible color changes in various solutions. This may be due the consumption of the Ag^+ ions in the solutions and the excitation of the surface plasmon resonance (SPR) effect [68]. The optical phenomenon observed in metal NPs is a distinctive effect that can be readily observed under UV-vis light, originating from the surface plasmon oscillation of free electrons [69]. AgNPs synthesized from plant-based extracts exhibit strong changes in color after incubation [70]. An intense brown color was also observed in aqueous leaf extracts from *B. prionitis* [10].

The highest percentage yield of the synthesized AgNPs from *B. albostellata* was obtained from the powdered stems solution (0.50%), followed by 0.32% from the methanolic leaf AgNPs (Table 1). The lowest percentage yield was obtained from NPs from the fresh stem solution (0.10%). Overall, this suggests that the percentage yield of phytocompounds in *B. albostellata* were greater in the leaf extract than the stem extract (Figure 1). NP yield can be affected by several factors, such as the type of material used, temperature, incubation time, amount of phytocompounds and metals present in the extracts used for the synthesis [16,71]. AgNPs obtained from the various extracts were characterized by UV-vis spectroscopy (Figure 2) and major peaks were distributed along the absorption band of the SPR [68]. Characteristic absorption peaks were observed at 416 nm (methanol leaves), 402 nm (methanol stems), 400 nm (fresh leaves), 398 nm (fresh stems), 450 nm (powdered leaves), and 438 nm (powdered stems), respectively. In previous literature, AgNPs have exhibited a maximum absorption in the range of 400–450 nm [72,73]. Plasmon bands are extended in Figure 2 with an absorption tail at longer wavelengths, which may be associated with the distribution and size of NPs [17]. Pirtarighat et al. [2] have suggested broad plasmon bands found in a specific spectrophotometric range that may be linked to the occurrence of different metabolites in the synthesized AgNPs from the plant extract. AgNPs produced from the leaf and stem solutions had a maximum absorbance of 4.00 a.u. (Figure 2). AgNPs synthesized from *B. longiflora* and *B. cristata* leaf extracts displayed a maximum absorption at 443 nm and 449 nm, respectively [60], while synthesis using aqueous leaf extracts of *B. prionitis*, produced a maximum absorption at 420 nm [10].

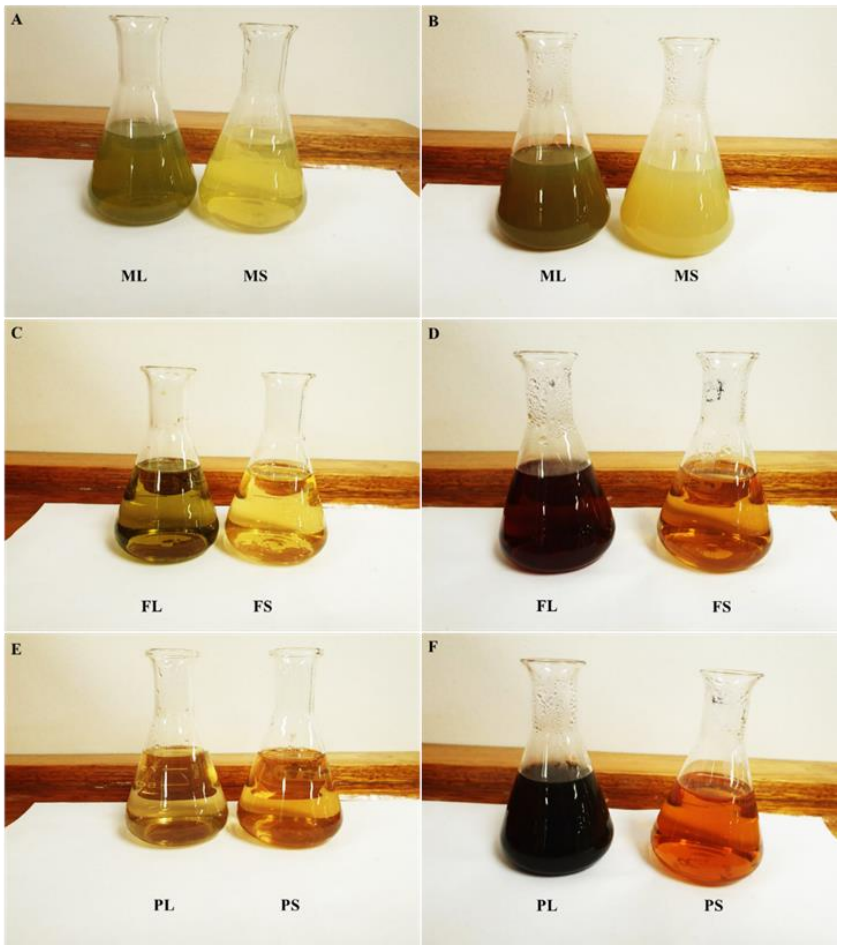

Figure 1. Silver nanoparticles synthesized from *B. albostellata* leaf and stem extracts: (**A**) Leaf and stem methanolic extracts before AgNP synthesis; (**B**) Leaf and stem methanolic extracts after incubation with $AgNO_3$; (**C**) Fresh leaf and stem extracts before AgNP synthesis; (**D**) Fresh leaf and stem extracts after incubation with $AgNO_3$; (**E**) Powdered leaf and stem extracts before AgNP synthesis; (**F**) Powdered leaf and stem extracts after incubation with $AgNO_3$.

Table 1. Percentage yield of the leaf and stem synthesized extracts of *B. albostellata*.

Crude Extract	Leaves	Stem	Leaves	Stem
	Dried AgNPs Yield (g)		Percentage Yield (%)	
Methanol	0.032	0.030	0.32	0.30
Fresh	0.030	0.010	0.12	0.04
Powdered	0.026	0.050	0.26	0.50

3.2. Scanning Electron Microscopy and EDX Analysis

Synthesized AgNPs from the various extracts exhibited dispersion throughout the samples with some level of agglomeration (Figure 3A,C, Figure 4A,C and Figure 5A,C). MubarakAli et al. [74] have reported that this could be due to a dehydration-induced aggregation of AgNPs. The spherical shape of nano-sized (<100 nm) AgNPs was confirmed by micrographs (Figure 3A,C, Figure 4A,C and Figure 5A,C). Similarly, previous reports on synthesized AgNPs from *B. prionitis* [10] and *B. cristata* [75] have highlighted their predominantly spherical morphology. All prepared samples for SEM analysis displayed considerable NP agglomeration, thus SEM micrographs were not ideal for assessing NP size. Gomathi et al. [75] have suggested that AgNPs synthesized from the leaf extracts of *B. cristata* were agglomerated because the biological constituents may have gathered smaller particles, forming larger knobs.

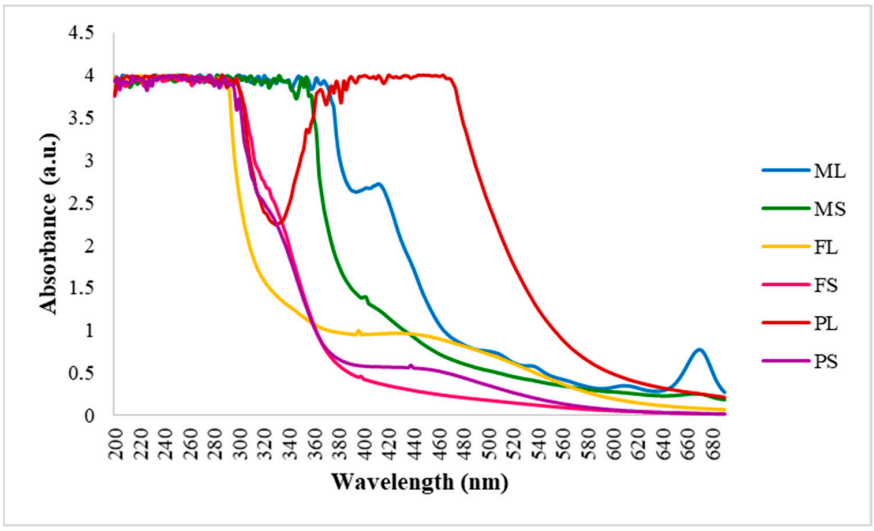

Figure 2. UV-visible spectroscopy of AgNPs synthesized from methanol, fresh and powdered leaves, and stem extracts of *B. albostellata* after 3 h incubation with $AgNO_3$. ML = Methanol leaf; MS = Methanol stem; FL = Fresh leaf; FS = Fresh stem; PL = Powdered leaf; PS = Powdered stem.

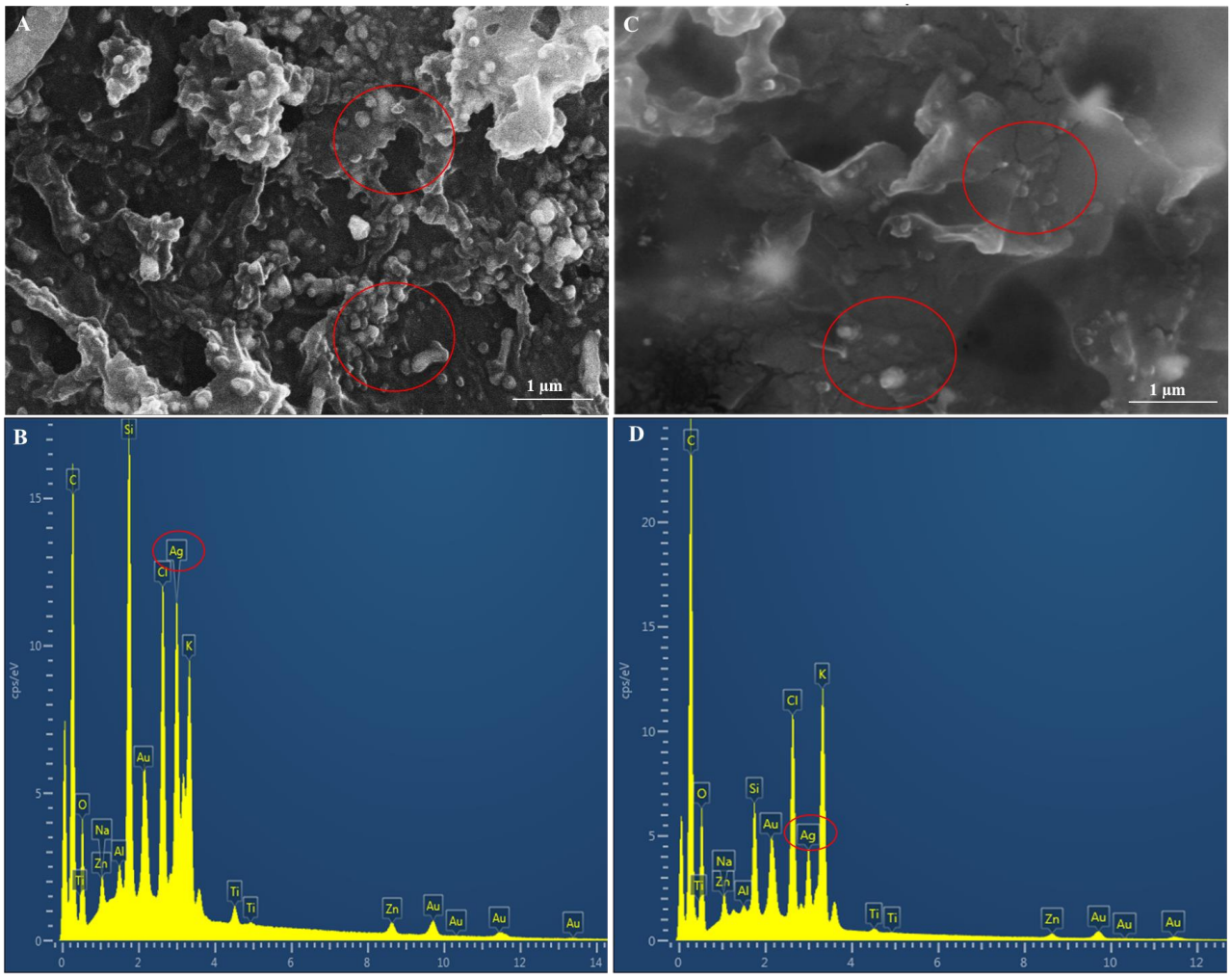

Figure 3. Micrographs of AgNPs synthesized from the methanol leaf extracts (**A**,**B**) and stem extracts (**C**,**D**) of *B. albostellata*. (**A**,**C**) Aggregated AgNPs; (**B**,**D**) EDX spectroscopy. Circles indicate AgNP agglomeration.

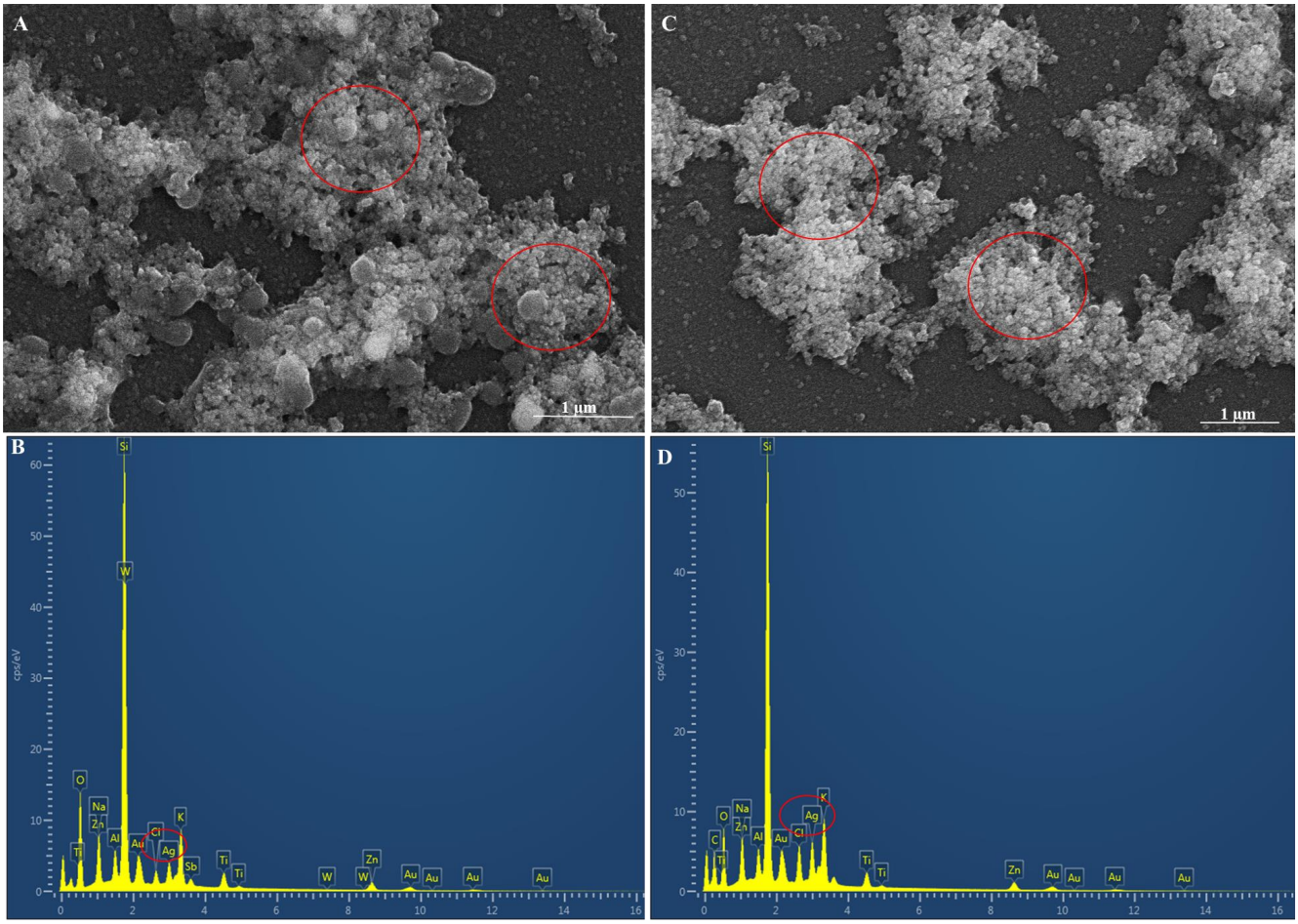

Figure 4. Micrographs of AgNPs synthesized from the fresh leaf extracts (**A**,**B**) and fresh stem extracts (**C**,**D**) of *B. albostellata*. (**A**,**C**) Aggregated AgNPs; (**B**,**D**) EDX spectroscopy. Circles indicate AgNP agglomeration.

EDX confirmed the presence of AgNPs and displayed strong peaks at 3 keV (Figure 3B,D, Figure 4B,D and Figure 5B,D). These peaks confirmed the biosynthesis of AgNPs and the organic compounds which were present on the NPs [76]. AgNPs synthesized from the leaf extracts of *B. prionitis* also displayed strong peaks at 3 keV [10]. Several studies have confirmed the presence of Ag^+ by observing the energy peak at 3 keV [77,78]. Overall, AgNPs from the methanolic leaf solution (Figure 3B) displayed the highest percentage of elemental Ag^+ ions (16.87 ± 0.89) and the lowest was found in the powdered stems (7.13 ± 1.44%) (Table 2). AgNPs from the methanolic stems had the second highest percentage of 14.78 ± 3.53. Fresh leaves and stems displayed Ag^+ ions at 9.47 ± 1.38% and 8.12 ± 0.71%, while the powdered leaf and stem material exhibited percentages at 8.85 ± 1.09 and 7.13 ± 1.44, respectively (Table 2). Kumar et al. [79] have proposed that different plant parts vary in their content of biochemical constituents, thus affecting the synthesis, size, and shape of AgNPs. The higher biosynthesized AgNPs obtained using leaf extracts (relative to the stems) may be due to their high concentration of secondary metabolites, as opposed to the stems, which may promote metal ion reduction [80].

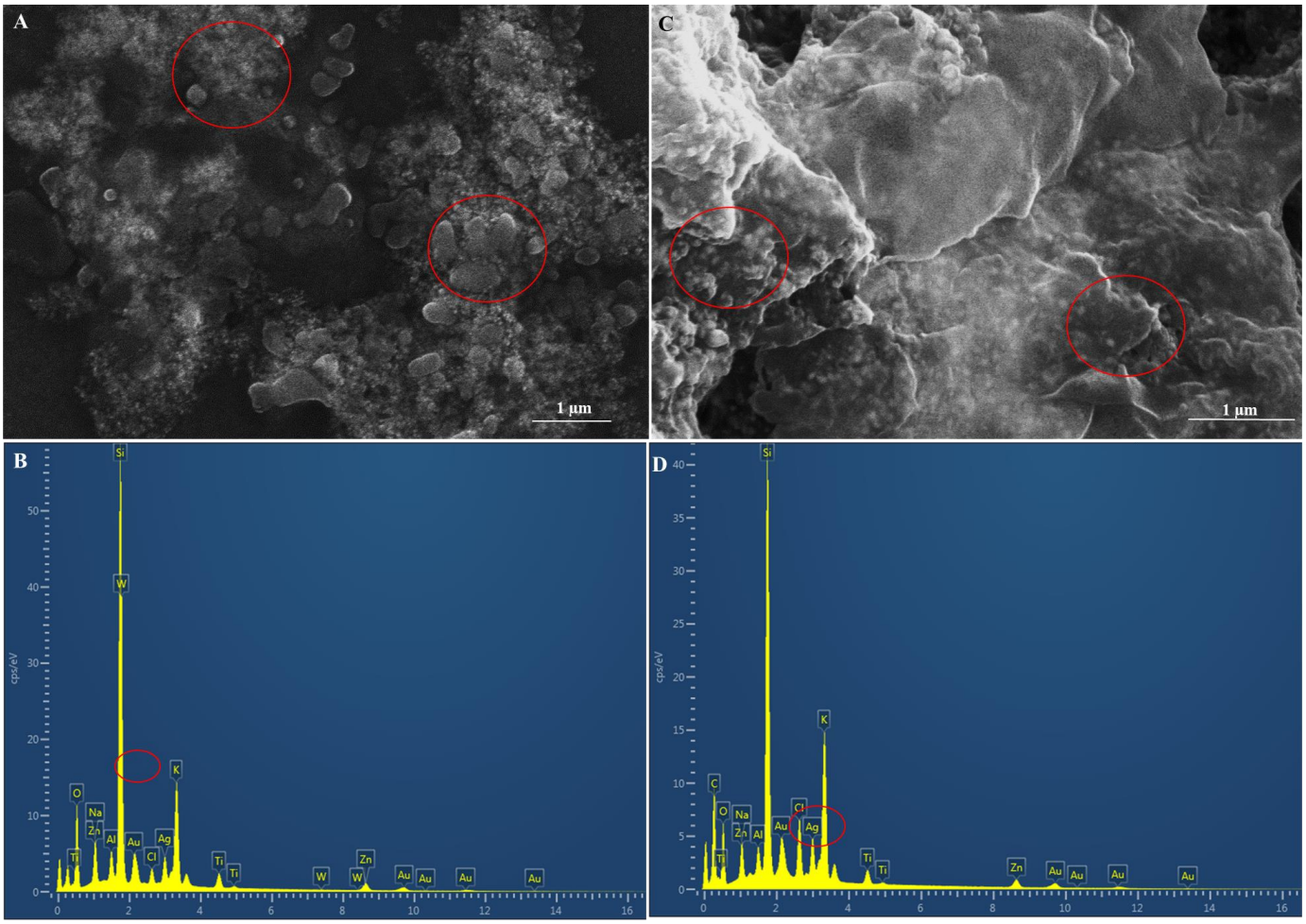

Figure 5. Micrographs of AgNPs synthesized from the powder leaf extracts (**A**,**B**) and powder stem extracts (**C**,**D**) of *B. albostellata*. (**A**,**C**) Aggregated AgNPs; (**B**,**D**) EDX spectroscopy. Circles indicate AgNP agglomeration.

Table 2. Average % weight of AgNPs synthesized from various leaf and stem extracts of *B. albostellata*.

Type of Extract	Average % Weight
Methanol leaf	16.87 ± 0.89
Methanol stem	14.78 ± 3.53
Fresh leaf	9.47 ± 1.38
Fresh stem	8.12 ± 0.71
Powdered leaf	8.85 ± 1.09
Powdered stem	7.13 ± 1.44

Data displayed as mean ± SD of triplicate.

3.3. High-Resolution Transmission Electron Microscopy of Synthesized AgNPs

Structural characteristics of the synthesized AgNPs were examined using HRTEM. NPs were evenly dispersed and occasionally detected either in clusters or merging into nano-clusters. The slight aggregation could be attributed to the elevated surface energy typically encountered during the preparation of NPs in an aqueous medium [81]. NPs synthesized from extracts of both leaf and stem (Figure 6) exhibited a small, generally spherical shape. Some NPs displayed either a spherical or triangular morphology. This variability in shape could be linked to distinct sets of phytochemicals that facilitate the reduction and stabilization of the AgNPs [82]. The kinetic energy of molecules increases at higher temperatures. This reaction speeds up the Ag ion consumption, thus reducing

the likelihood for particle size development [83]. This could explain the small particle size found in the HRTEM micrographs.

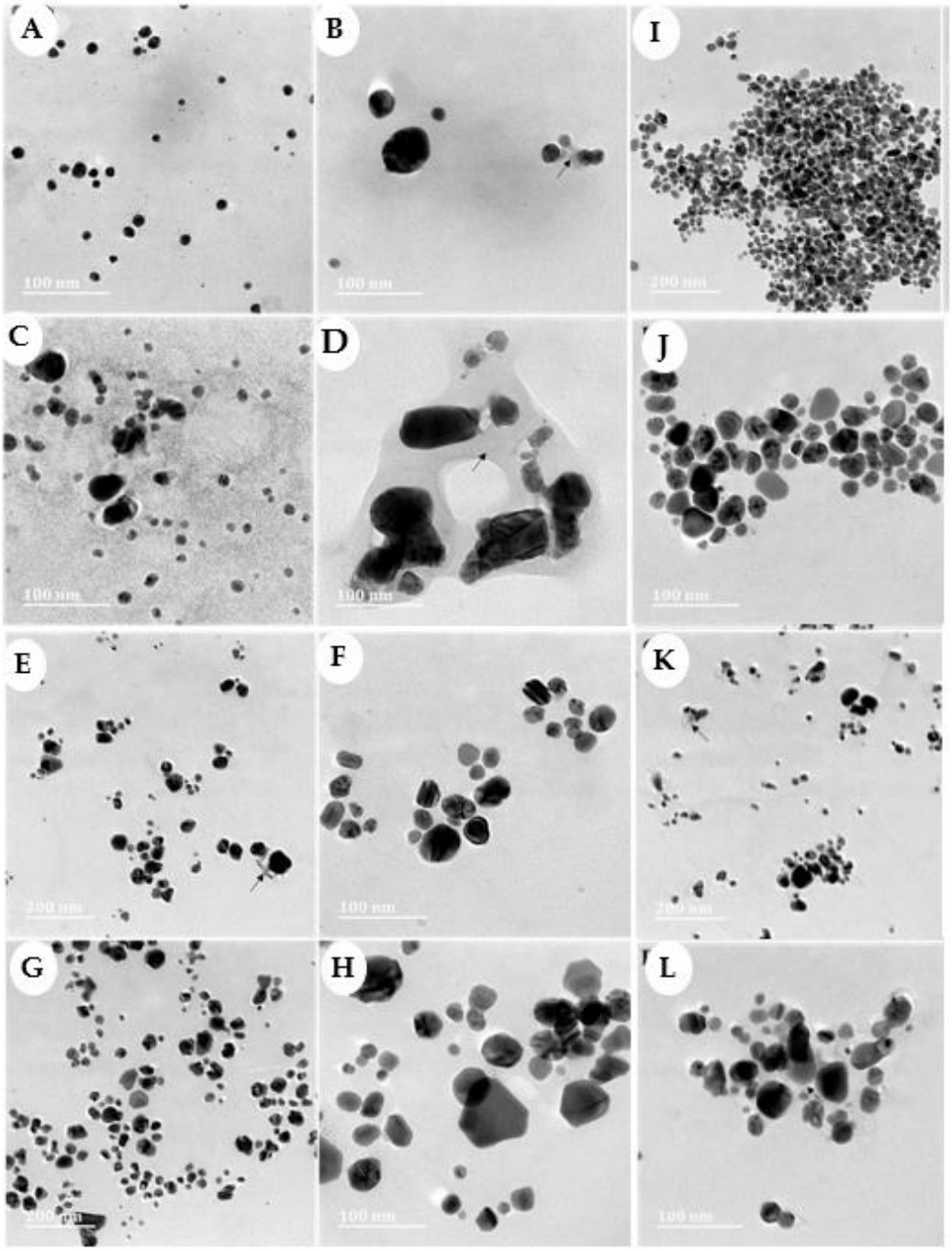

Figure 6. HRTEM micrographs of the AgNPs synthesized from (**A**,**B**) methanolic leaf extracts; (**C**,**D**) methanolic stem extracts, (**E**,**F**) fresh leaf extracts; (**G**,**H**) fresh stem extracts, and (**I**,**J**) powdered leaf extracts; (**K**,**L**) powdered stem extracts of *B. albostellata*. Arrowhead indicates film around AgNPs.

Verma and Mehata [83] have proposed that the size of AgNPs can be modified by manipulating pH levels, concentration, and temperature. A thin film layer was observed surrounding the AgNPs in both leaf and stem extracts (Figure 6B,D). Mallikarjuna et al. [84] have detected similar films around synthesized AgNPs and recognized this as AgNPs capping the functional groups. Cittrarasu et al. [61], have validated this observation by identifying comparable films in the aqueous leaf extracts of *B. longiflora*, proposing that

the thin layer constituted the organic material capping the AgNPs. Furthermore, Mittal et al. and Restrepo and Villa [85,86] have suggested that the functional group's capping might enhance the stability of AgNPs in the solution. According to the histogram for mean particle size, AgNP sizes were not uniform and varied across the different extracts (methanolic leaves and stems (Figure 7A,B)), (aqueous fresh leaves and stems (Figure 7C,D)), (and aqueous powdered leaves and stems (Figure 7E,F)) from *B. albostellata*, However, all particles were below 100 nm. The sizes of synthesized NPs from the leaf and stem extracts were as follows: 31.69 nm (Figure 6A), 34.32 nm (Figure 6B), 21.77 nm (Figure 6C), 20.48 nm (Figure 6D), 18.39 nm (Figure 6E), and 16.57 nm (Figure 6F), respectively. AgNPs of a similar size (15–30 nm) have been observed in *B. cristata* [75]. Additionally, spherical NPs synthesized from the aqueous leaf extracts of *B. prionitis* varied from 10 to 20 nm [10].

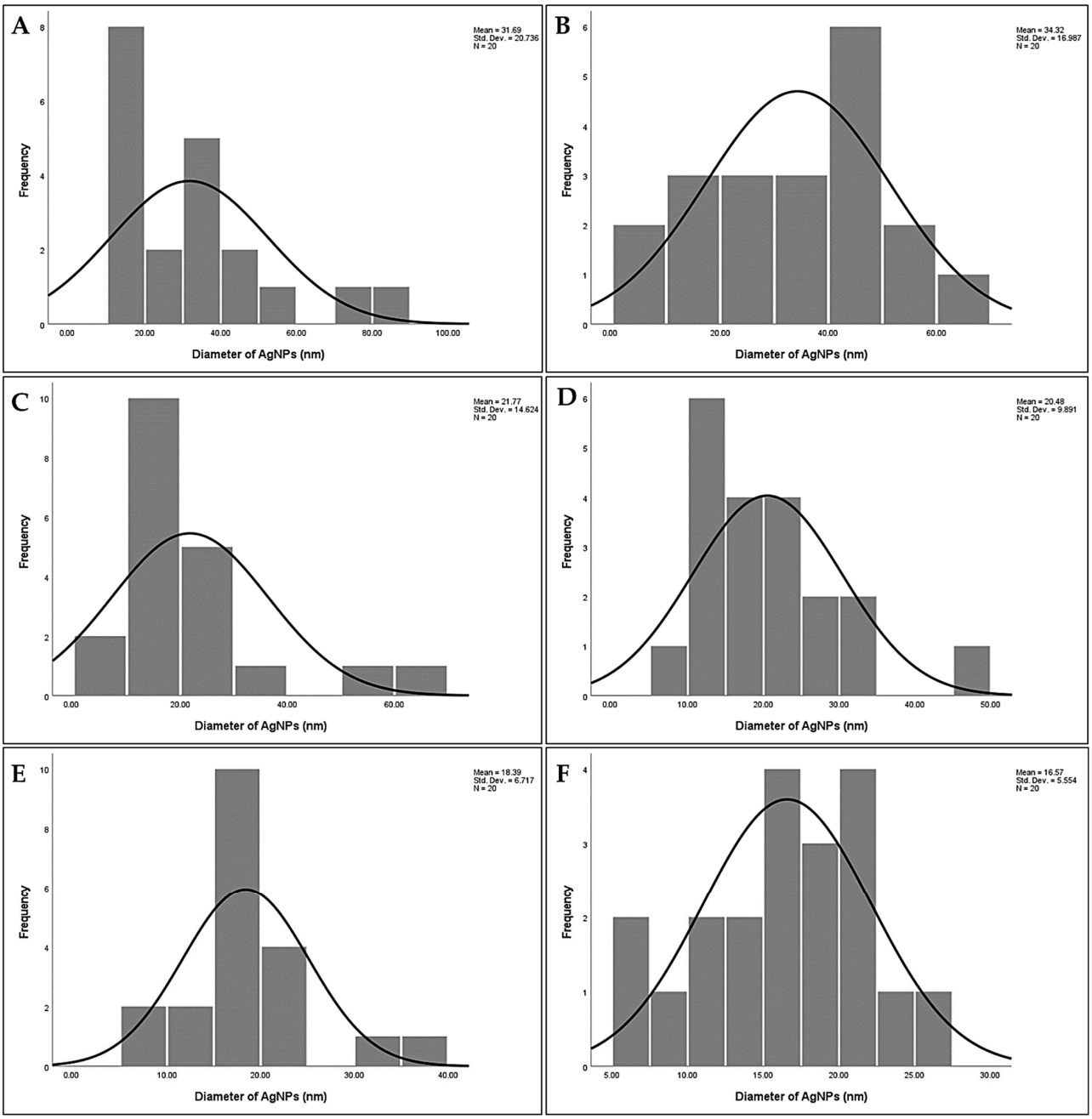

Figure 7. The mean particle size of synthesized AgNPs. (**A**) methanolic leaf extracts; (**B**) methanolic stem extracts; (**C**) aqueous fresh leaf extracts; (**D**) aqueous fresh stem extracts; (**E**) powdered leaf extracts; (**F**) powdered stem extracts of *B. albostellata*.

The mean particle size in Figure 7A is right skewed; this means that the size of the majority of the AgNPs from the methanolic leaf extracts were between 20–40 nm. Additionally, the mean particle size in Figure 7B,F is left skewed, with a large portion of the data on the right, and smaller observations trailing off to the left. In Figure 7C,D, the mean particle size is right skewed, with the majority set off to the left, while a few observations are trailing off to the right. Figure 7E displays the mean particle size that appeared almost bell-shaped, with a large peak in the middle and tails that extend on either side at nearly the same frequency.

3.4. Nanoparticle Tracking Analysis (NTA)

NTA was utilized to precisely determine the size and distribution of the AgNPs, their colloidal stability, and their zeta potential (Table 3). These results indicated that the AgNPs synthesized from the methanolic leaf and stem extracts had a mean diameter of 111.3 ± 4.4 nm and 110.7 ± 4.2 nm, which contradicts the HRTEM results. As stated previously, various sizes of the synthesized AgNP solutions were visualized using HRTEM and measured using imageJ 1.53 e analysis. However, the sizes and zeta potential of the AgNPs, as well as their complexes, were evaluated using NTA. The differences in results may be due to the fact that, during HRTEM analysis, AgNP solutions of the various extracts were pipetted onto copper grids, dried with the aid of a UV lamp and thereafter visualized. Nonetheless, NTA involves the preparation of solutions in an aqueous suspension for analysis, yielding a hydrodynamic diameter more akin to what is expected in a biological system. It has been reported that sizes obtained from NTA are expectedly slightly larger than that observed under TEM [86,87]. The zeta potential of a solution is regarded as the electrostatic value of the nanoparticle, and this then correlates to the surface charge of nanoparticles [88].

Table 3. Size distribution and zeta potential analysis of AgNPs synthesized from various extracts.

Sample (AgNPs)	Nanoparticle Size (nm) (Mean + Standard Error)	Zeta Potential (mV) (Mean + Standard Error)
Methanol leaf	111.3 ± 4.4	−33.2 ± 0.1
Methanol stem	110.7 ± 4.2	−28.2 ± 0.0
Fresh leaf	53.9 ± 8.4	−8.8 ± 0.2
Fresh stem	37.7 ± 0.9	−17.2 ± 0.0
Powdered leaf	57.9 ± 0.6	−17.0 ± 0.0
Powdered stem	34.3 ± 0.2	−16.8 ± 0.1

Zeta potential has been commonly used by the pharmaceutical industry to evaluate their formulations for stability. A desirable zeta potential value of less than −30 mV or greater 30 mV is usually considered to have adequate repulsive force in order to achieve improved physical colloidal stability [89]. A zeta potential within this range is regarded as stable, owing to the substantial mobility within the solution, and greater levels of electrostatic repulsion, thereby reducing NP aggregation [90]. Conversely, a minute zeta potential value could lead to the aggregation or flocculation of NPs due to the influence of van der Waals attractive forces, resulting in the physical instability of the NPs [91–93]. The zeta potential of a sample is influenced by two key factors: the pH and the conductivity of the solution in which the NPs are dispersed [94]. AgNPs synthesized from the leaf and stem methanolic extracts exhibited a high zeta potential of −33.2 ± 0.1 and −28.2 ± 0.0, respectively (Table 3). This indicates good long-term colloidal stability and potential suitability for in vivo application. The lowest zeta potential was observed in the AgNPs synthesized from the fresh leaf extracts (−8.8 mV).

3.5. Fourier-Transform Infrared Spectroscopy of Synthesized AgNPs

The FTIR spectroscopy of synthesized AgNPs using the leaves and stems are presented in Figures 8–10, respectively. Prominent peaks were observed for the methanolic leaf

extracts at 3273.31, 2927.50, 2346.67, 2119.29, 1622.25, 1393.67, 1333.55, 1287.63, 1034.01, 897.23, 813.23 cm^{-1} (Figure 8A) and stems at 3330.48, 3276.33, 2347.91, 2119.13, 1619.30, 1474.26, 1392.44, 1332.30, 1041.01, 932.56, 895.77 cm^{-1} (Figure 8B). Additionally, for the aqueous fresh leaf extracts, peaks were observed at 3397.89, 3370.78, 2331.58, 2122.09, 1911.28, 1599.40, 1389.56, 1323.17, 1070.81, 1039.08, 820.01, 722.42 cm^{-1} (Figure 9A) and stems at 3269.77, 2929.85, 2348.90, 2110.30, 2094.08, 1614.30, 1391.17, 1330.95, 1038.69, 896.38, 821.34 cm^{-1} (Figure 9B). Lastly, peaks for the aqueous powdered leaf extracts were detected at 3281.52, 3223.08, 2927.53, 2328.14, 2115.65, 1888.35, 1592.68, 1394.61, 1336.86, 1036.22, 808.04, 767.36 cm^{-1} (Figure 10A) and stems at 3262.30, 2929.28, 2344.39, 2116.90, 1607.25, 1391.95, 1333.34, 1036.10, 766.74 cm^{-1} (Figure 10B).

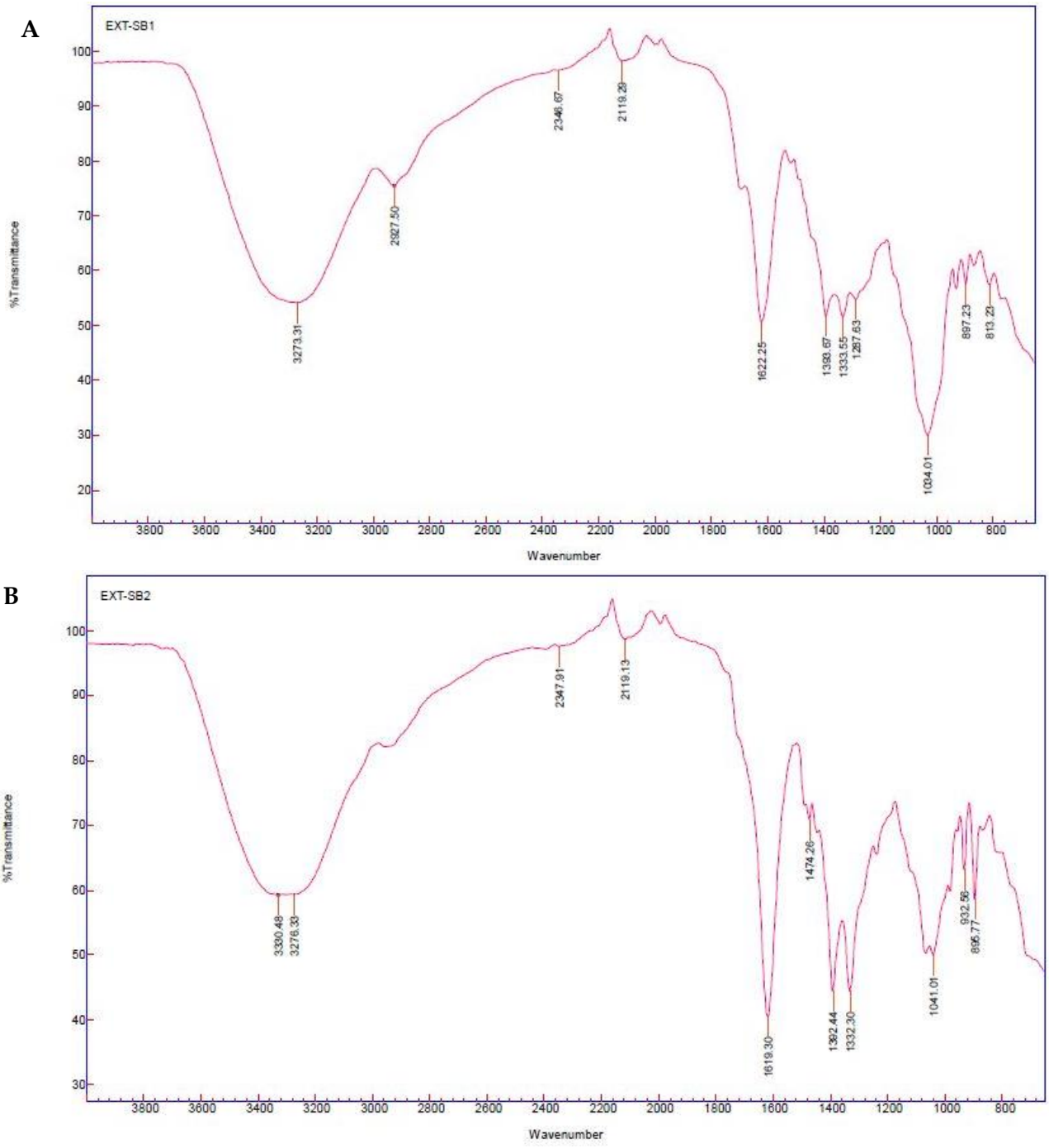

Figure 8. FTIR spectra of synthesized AgNPs synthesized. (**A**) leaf methanolic extracts; (**B**) Stem methanolic extracts of *B. albostellata*.

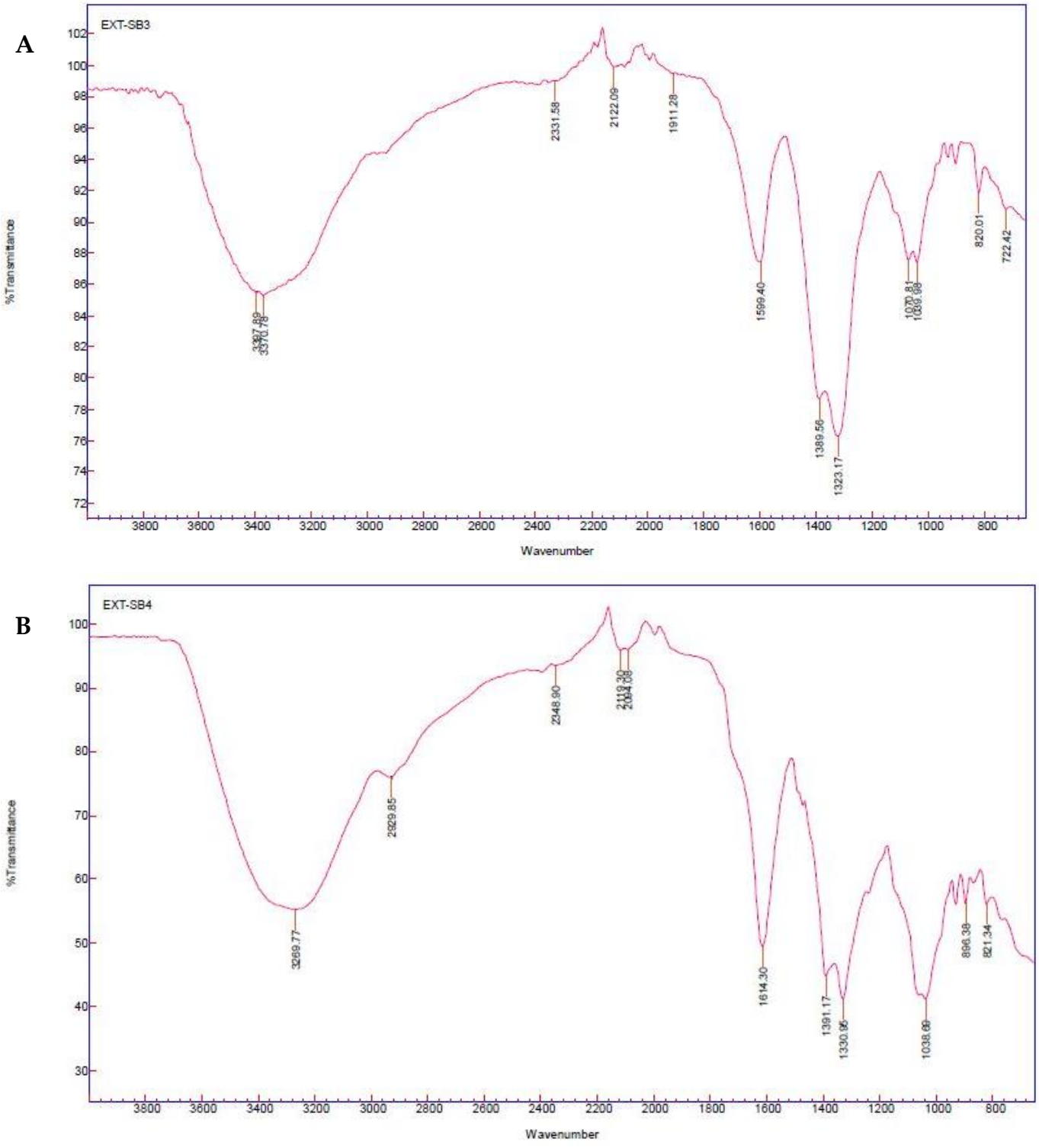

Figure 9. FTIR spectra of the synthesized AgNPs. (**A**) aqueous fresh leaf extracts; (**B**) aqueous fresh stem extracts of *B. albostellata*.

Absorbance peaks observed between 2700–3200and 3200–3550 cm^{-1} are distinctive to a possible O-H stretching group of polyphenols/alcohol, respectively [95–97]. A peak at 3330.48 cm^{-1} corresponds to phenolic hydroxyl groups and secondary amines. A similar peak has been observed in *B. longiflora* leaf aqueous extract [61]. The presence of a moderately sharp peak at 2927 cm^{-1} was associated with the asymmetric vibration of methylene groups C–H (methoxy compounds) [98]. The 2117 and 2120 cm^{-1} wavelengths

display the symmetrical C≡C vibration of alkynes. Bands appearing in the range of 1700–1600 cm^{-1} were linked to C–O stretching vibrations [99]. Bands at 1619.30 and 1622.25 cm^{-1} were characteristic to C=O stretching. A band at 1619 cm^{-1} was designated to flavonoid and fisetin [100].

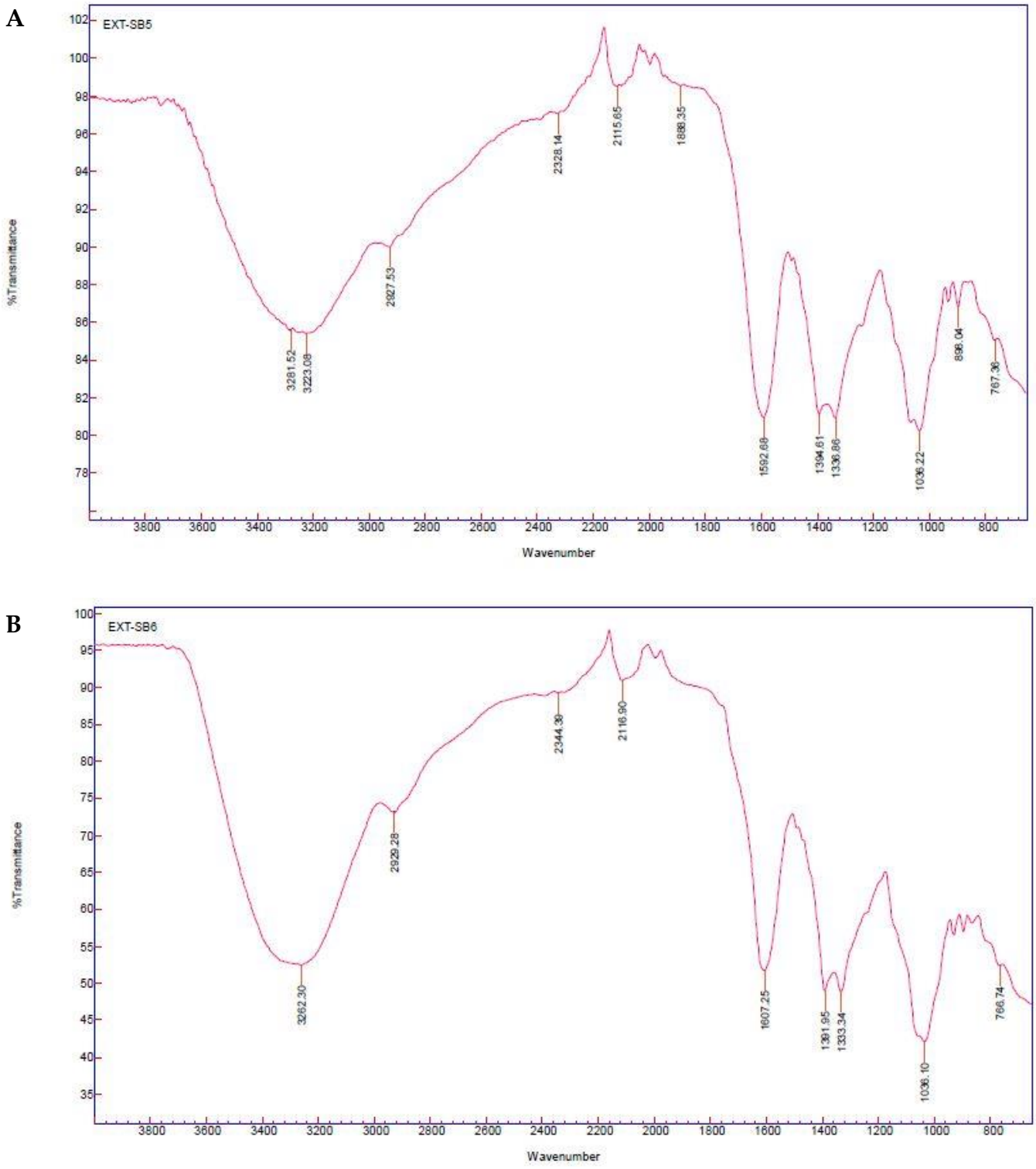

Figure 10. FTIR spectra of the synthesized AgNPs. (**A**) powdered leaf extracts; (**B**) powdered stem extracts of *B. albostellata*.

Peaks at 1650–1580 cm^{-1} may be linked to symmetric N-H bending (amine). Similar bending vibrations related to amine were observed in the leaf extracts of *B. prionitis* [10], while peaks at 1420–1330 cm^{-1} were related to O-H bending. Bands ranging from 1390–1380 cm^{-1} are characteristic to C-H bending of aldehyde. Aromatic amine, C-N stretching is related to peaks at 1342–1266 cm^{-1}. Aromatic esters are associated to the symmetric vibration C-O at peaks of 1310–1250 cm^{-1}. Additionally, vibrational stretching of C-O was observed in the leaf extracts of *B. prionitis* [10]. Peaks at 1250–1020 cm^{-1} relate to the symmetric C–N vibration of amine [101]. Peaks at 850–550 cm^{-1} are linked to C-Cl stretching, a halo compound. Peaks in the range of 880 ± 20 cm^{-1} and 810 ± 20 cm^{-1} corresponds to C-H bending. A peak at 755 ± 20 cm^{-1} represents C-H bending (1,2-disubstituted). Ghosh et al. [10] have reported the extensive phytochemical variety found in the leaf extracts of *B. prionitis*, which included phenols, ascorbic acid, citric acid, and reducing sugars, among other compounds that could potentially contribute significantly to the reduction and stabilization of AgNPs. The majority of absorbance bands observed in the synthesized extracts of *B. albostellata* displayed distinctive functional groups such as phenols, alcohols, terpenes, alkynes, aldehydes, primary, and secondary amines. Hence, the phyto-constituents existing in the *B. albostellata* leaves and stems evidently displayed an important role in the bioreduction process of the synthesized AgNPs.

The FTIR frequencies observed showed the occurrence of several functional groups (Table 4). Phenolic compounds were detected in the stem methanol, fresh leaves, fresh stems, and powdered leaves. The above results suggest that the observed AgNP capping may contain terpenoids and phenolic compounds, with several functional groups alcohols, carboxylic acids, and esters etc. These compounds could have been impacted by the various treatments used (ratios of leaf and stem material and different solvents), which may have reduced $AgNO_3$ to AgNPs by means of several bioactive compounds [102]. Furthermore, the presence of impurities may be linked to the presence of other organic substances in the different plant extracts [103].

Table 4. FTIR spectral frequencies of synthesized AgNPs using extracts of *B. albostellata*.

Plant Extract	Absorption Frequency (cm^{-1})	Types of Absorption/ Vibration	Functional Group	Compound Class
Leaf methanol	3273.31	Stretch	O-H	Alcohol
	2927.50	Stretch	C–H	Alkane
	2346.67	Stretch	O=C=O	Carbon dioxide
	2119.29	Symmetrical	C≡C	alkynes
	1622.25	Stretch	C=C	Conjugated alkene
	1393.67	Bending	C–H	Aldehyde
	1333.55	Bending	O-H	Alcohol
	1287.63	Stretch	N-O	Nitro
	1034.01	Stretch	S=O	sulfoxide
	897.23	Bending	C=C	Alkene
	813.23	Bending	C=C	Alkene

Table 4. *Cont.*

Plant Extract	Absorption Frequency (cm^{-1})	Types of Absorption/ Vibration	Functional Group	Compound Class
Stem methanol	3330.48	Stretch	N-H	Aliphatic primary amine
	3276.33	Stretch	O-H	Alcohol
	2347.91	Stretch	O=C=O	Carbon dioxide
	2119.13	Stretch	N=C=N	Carbodiimide
	1619.30	Stretch	C=C	α,β-unsaturated ketone
	1474.26	Bending	C-H	Alkane
	1392.44	Bending	O-H	Phenol
	1332.30	Stretch	C-N	Aromatic amine
	1041.01	Stretch	CO-O-CO	Anhydride
	932.56	Bending	C=C	Alkene
	895.77	Bending	C=C	Alkene
Fresh leaf	3397.89	Stretch	N-H	Aliphatic primary amine
	3370.78	Stretch	N-H	Aliphatic primary amine
	2331.58	Stretch	O=C=O	Carbon dioxide
	2122.09	Stretch	N=C=S	Isothiocyanate
	1911.28	Bending	C-H	Aromatic compound
	1599.40	Stretch	N-O	Nitro compound
	1389.56	Bending	O-H	Phenol
	1323.17	Stretch	C-N	Aromatic amine
	1070.81	Stretch	S=O	sulfoxide
	1039.08	Stretch	S=O	sulfoxide
	820.01	Bending	C=C	Alkene
	722.42	Bending	C=C	Alkene
Fresh stem	3269.77	Stretch	O-H	Carboxylic acid
	2929.85	Stretch	C-H	Alkane
	2348.90	Stretch	O=C=O	Carbon dioxide
	2110.30	Stretch	N=C=S	Isothiocyanate
	2094.08	Stretch	N=C=S	Isothiocyanate
	1614.30	Stretch	C=C	α,β-unsaturated ketone
	1391.17	Stretch	C-F	Fluoro compound
	1330.95	Bending	O-H	Phenol
	1038.69	Stretch	S=O	Sulfoxide
	896.38	Bending	C=C	Alkene
	821.34	Bending	C=C	Alkene

Table 4. *Cont.*

Plant Extract	Absorption Frequency (cm^{-1})	Types of Absorption/ Vibration	Functional Group	Compound Class
Powdered leaf	3281.52	Stretch	O-H	Alcohol
	3223.08	Stretch	O-H	Carboxylic acid
	2927.53	Stretch	N-H	Amine salt
	2328.14	Stretch	O=C=O	Carbon dioxide
	2115.65	Stretch	N=C=S	Isothiocyanate
	1888.35	Bending	C-H	Aromatic compound
	1592.68	Bending	N-H	Amine
	1394.61	Stretch	C-F	Fluoro compound
	1336.86	Bending	O-H	Phenol
	1036.22	Stretch	C-N	Amine
	808.04	Stretch	C-Cl	Halo compound
	767.36	Stretch	C-Cl	Halo compound
Powdered stem	3262.30	Stretch	O-H	Alcohol
	2929.28	Stretch	N-H	Amine salt
	2344.39	Stretch	O=C=O	Carbon dioxide
	2116.90	Stretch	N=C=S	Isothiocyanate
	1607.25	Bending	N-H	Amine
	1391.95	Stretch	C-F	Fluoro compound
	1333.34	Bending	O-H	Alcohol
	1036.10	Stretch	C-N	Amine
	766.74	Stretch	C-Cl	Halo compound

3.6. Antibacterial Activity of Synthesized AgNPs from Various Leaf and Stem Extracts

The use of AgNPs in antibacterial assays is a fascinating strategy to overcome the problem of multidrug resistance by bacteria [104]. AgNPs synthesized from leaf and stem extracts were subjected to antibacterial analysis. Various concentrations (100, 50, 25, 12.25, 6.25, and 3.125 mg/mL) were tested against Gram-positive and Gram-negative strains of bacteria. Clear zones of inhibition were observed for the AgNPs synthesized from the leaf and stem methanolic, and fresh and powdered extracts against Gram-positive *B. subtillus*, methicillin-resistant *S. aureus*, *S. aureus* and Gram-negative *E. coli* and *P. aeruginosa*. The highest inhibitory activity was observed at 100 mg/mL in all AgNPs, for both Gram-positive and Gram-negative bacteria. From all of the AgNPs tested against *B. subtillus*, the NPs from the fresh stem displayed the highest inhibitory activity (18.33 ± 3.21 mm), while the lowest was observed in the powdered leaf (12.33 ± 1.53 mm) (Table 5). No inhibitory activity was observed in the leaf and stem AgNPs at 6.25 and 3.125 mg/mL against *B. subtillus* (Table 4). The powdered stem AgNPs displayed the highest activity (18.67 ± 3.21 mm) against Methicillin-resistant *S. aureus*, while the fresh leaf AgNPs demonstrated the lowest (12.00 ± 2.65 mm) (Table 5). Only the powdered leaf AgNPs at 6.25 mg/mL displayed no activity against Methicillin-resistant *S. aureus*. No observed activity was observed at 3.125 mg/mL against Methicillin-resistant *S. aureus* (Table 5). The methanolic leaf AgNPs showed the highest inhibitory activity against *S. aureus* (16.67 ± 2.52 mm), whereas the powdered leaf AgNPs displayed the lowest (13.67 ± 2.52 mm). In *S. aureus*, no zones

of inhibition were observed at 6.25 and 3.125 mg/mL for both powdered leaf and stem methanolic AgNPs (Table 5). Furthermore, at 3.125 mg/mL, the powdered stem AgNPs displayed no activity against *S. aureus* (Table 5). The powdered stem AgNPs demonstrated the highest activity (19.33 ± 1.15 mm) against *E. coli*, whereas the powdered leaf AgNPs showed the lowest activity (15.00 ± 1.00 mm). Zones of inhibition were observed at all concentrations for all AgNPs against *E. coli* (Table 5). Furthermore, Gangaram et al. [56] have evaluated the antibacterial activity of the crude leaf and stem extracts (hexane, chloroform and methanol). These authors found the antibacterial activity of the crude leaf methanolic extract at 100 mg/mL had the highest inhibition against all tested bacterial strains. Whereas, the crude stem methanolic extracts had the highest inhibition against *S. aureus* and *P. aeruginosa* only. According to the HRTEM analysis, AgNPs synthesized from the various extracts ranged from 34.32–16.57 nm. Numerous studies have reported that AgNPs of smaller dimensions (<30 nm) have a greater ability to penetrate into bacteria [105,106]. This suggests that smaller particles may engage with the contact surface of bacteria more frequently than larger ones, therefore improving their antibacterial activity [107,108]. Additionally, the morphology and physicochemical characteristics of NPs have been recognized to exert an effect on their antimicrobial activities [109,110]. Kvitek et al. [111] have found smaller size AgNPs to display greater surface area then the larger particles, resulting in improved antibacterial activity. This was further validated by Collins et al. [112], who have suggested that small-sized particles exhibit strong antibacterial activity, due to their enhanced capacity to penetrate bacterial cells.

Table 5. Antibacterial activity of synthesized AgNPs from *B. albostellata* against human pathogenic strains (zone of inhibition mm).

Strain	Concentration (mg/mL)	Treatments/Synthesized AgNPs						Positive Control (mg/mL)	
		Leaf Methanol	Fresh Leaves	Powder Leaves	Stem Methanol	Fresh Stem	Powder Stem	L	S
BS	3.125	R	R	R	R	R	R	9.00 ± 1.00	11.00 ± 1.00
	6.25	R	R	R	R	R	R		
	12.5	6.67 ± 0.58	7.33 ± 0.58	6.67 ± 0.58	6.67 ± 0.58	6.67 ± 1.15	7.00 ± 0.00		
	25	7.33 ± 0.58	8.00 ± 1.00	8.00 ± 1.00	7.67 ± 1.15	8.00 ± 1.73	9.00 ± 0.00		
	50	9.67 ± 2.08	9.67 ± 3.79	10.00 ± 1.73	9.00 ± 3.46	9.33 ± 2.31	11.33 ± 2.31		
	100	13.33 ± 3.06	14.33 ± 2.52	12.33 ± 1.53	15.00 ± 4.58	18.33 ± 3.21	17.33 ± 3.21		
MRSA	3.125	R	R	R	R	R	R	9.33 ± 0.58	9.00 ± 1.00
	6.25	7.00 ± 1.73	6.67 ± 0.58	R	6.67 ± 0.58	6.67 ± 0.58	6.67 ± 0.58		
	12.5	9.33 ± 0.58	7.00 ± 0.00	6.00 ± 1.00	7.33 ± 1.15	7.67 ± 1.53	9.00 ± 1.00		
	25	10.67 ± 0.58	8.00 ± 1.00	7.33 ± 0.58	9.33 ± 1.15	9.67 ± 0.58	11.67 ± 1.53		
	50	12.67 ± 2.52	9.00 ± 1.00	10.00 ± 3.00	12.67 ± 2.52	12.00 ± 2.00	14.00 ± 4.00		
	100	14.67 ± 0.58	12.00 ± 2.65	11.00 ± 2.00	15.00 ± 1.00	14.00 ± 3.00	18.67 ± 3.21		
SA	3.125	7.33 ± 1.53	7.33 ± 0.58	R	R	6.67 ± 0.58	R	9.67 ± 0.58	10.00 ± 1.00
	6.25	9.00 ± 2.65	8.00 ± 6.93	R	R	7.33 ± 1.15	7.33 ± 1.53		
	12.5	10.33 ± 0.58	9.33 ± 3.05	7.33 ± 2.08	7.67 ± 1.52	8.67 ± 1.53	8.67 ± 0.58		
	25	11.67 ± 2.08	10.33 ± 0.58	9.67 ± 1.15	9.33 ± 1.15	10.33 ± 0.58	9.33 ± 2.52		
	50	15.00 ± 1.00	12.00 ± 1.00	11.67 ± 3.79	12.33 ± 3.06	13.33 ± 2.31	13.67 ± 2.52		
	100	16.67 ± 2.52	14.00 ± 2.65	13.67 ± 2.52	15.00 ± 2.65	16.00 ± 2.65	16.33 ± 4.72		
EC	3.125	7.00 ± 1.00	7.33 ± 0.58	7.00 ± 0.00	7.00 ± 0.00	8.33 ± 0.58	7.67 ± 0.58	8.67 ± 0.58	9.33 ± 0.58
	6.25	8.67 ± 0.58	9.33 ± 0.58	8.67 ± 0.58	9.33 ± 0.58	9.67 ± 0.58	9.33 ± 0.58		
	12.5	10.33 ± 0.58	11.33 ± 1.53	10.00 ± 0.00	10.33 ± 2.52	11.33 ± 0.58	10.67 ± 1.53		
	25	12.00 ± 2.65	13.67 ± 1.53	11.67 ± 0.58	12.33 ± 2.31	13.00 ± 2.65	12.33 ± 1.15		
	50	14.00 ± 2.65	14.00 ± 1.00	13.67 ± 4.16	14.00 ± 1.73	15.33 ± 0.58	14.00 ± 1.00		
	100	18.67 ± 3.51	15.67 ± 1.53	15.00 ± 1.00	16.67 ± 2.31	17.00 ± 3.00	19.33 ± 1.15		
PA	3.125	7.33 ± 1.53	7.00 ± 0.00	R	R	7.00 ± 0.00	7.00 ± 0.00	9.33 ± 0.58	8.67 ± 1.15
	6.25	8.33 ± 1.53	7.67 ± 1.15	7.00 ± 0.00	7.33 ± 0.58	8.33 ± 0.58	7.67 ± 0.58		
	12.5	13.00 ± 2.65	10.33 ± 3.51	8.67 ± 1.53	8.00 ± 1.73	11.67 ± 2.89	9.67 ± 0.58		
	25	14.33 ± 3.05	12.33 ± 2.08	10.67 ± 3.79	11.67 ± 2.89	13.33 ± 2.89	11.00 ± 3.00		
	50	15.33 ± 1.53	13.67 ± 3.21	13.67 ± 3.52	13.67 ± 3.21	14.67 ± 0.58	15.33 ± 0.58		
	100	21.67 ± 2.87	17.00 ± 1.00	15.00 ± 4.00	19.67 ± 1.53	17.33 ± 3.79	18.67 ± 1.15		

BS = *B. subtillus*, MRSA = methicillin-resistant *S. aureus*, SA = *S. aureus*, EC = *E. coli*, PA = *P. aeruginosa*, R = resistant, Positive controls (Streptomycin 10 mg/mL, Gentamicin 10 mg/mL), Negative control = DMSO, (n = 3).

Pirtarighat et al. [2] have proposed that the bactericidal activity of AgNPs is due to the attachment of these particles to the cell wall. Ag^+ ions released from NPs promote antibacterial activity. Additionally, these positively charged ions react with the phosphorus

and sulphur found in biomolecules such as DNA and RNA in the bacterial cells, thereby causing their disruption [113,114]. According to various reports in the literature, the antibacterial potential of AgNPs is observed in their ability to denature the outer membrane of bacteria [115]; cause gaps/pits in the membrane, resulting in their destruction [116,117]; and bring about an interaction between the AgNPs and sulfhydryl/disulphide groups of enzymes, hindering their metabolic processes and leading to cell death [118]. The potency of synthesized AgNPs from the leaves of *B. cristata* [75] and *B. gibsoni* [81] have showed antibacterial activity against *S. aureus* and *E. coli*. AgNPs are known to affect various biological processes within microorganisms, as they modify the structure and function of the cell membrane, rendering them permeable [119]. AgNPs were reported to accumulate on the membrane of *E. coli* cells, creating a gap in the integrity of the bilayer and increasing its permeability, resulting in bacterial cell death [75,120]. For *P. aeruginosa*, AgNPs from the leaf methanolic extract displayed the highest inhibitory activity (21.67 ± 2.87 mm), while the lowest was observed in the powdered AgNPs (15.00 ± 4.00 mm). Additionally, no observed activity was observed at 3.125 mg/mL in the powdered leaf and stem methanolic AgNPs against *P. aeruginosa* (Table 5). Cittrarasu et al. [61] have evaluated the antibacterial activity of AgNPs synthesized from *B. longiflora* aqueous leaf extracts. According to these authors, strong antibacterial activity at 100 mg/mL was observed against *S. aureus* (14.5 ± 0.08 mm) and *P. aeruginosa* (18 ± 0.14 mm). Therefore, the biosynthesized AgNPs from the leaves and stem extracts of *B. albostellata*, exhibited antibacterial activity against both Gram-positive and Gram-negative bacteria.

3.7. In Vitro Cytotoxic Effect on Cancerous Cell Lines Using Synthesized AgNPs

The preparation of NPs that can eradicate cancerous cells while leaving normal cells unharmed will be a crucial step towards improving harsh toxicities linked with drug administration. In vitro cytotoxicity analysis is a valuable tool for screening synthesized compounds with potential anti-cancer activity. The MTT assay evaluated the level of cell death. MTT is reduced in the mitochondria, and the absorbance measured is suggestive of the mitochondrial activity of the cell population, and hence the amount of viable cells [121]. As shown in Figure 11A–C, the percentage of cell survival for all synthesized extracts were dose-dependent. All AgNPs at various concentrations showed high cytotoxicity against all cell lines (Figure 11A–C). NPs can efficiently enter the tumor micro-environment and prevent cancer cells from metastasizing [122–124]. Controls 1, represented 100% of viable cells, while control 2 contained DMSO only. For HEK293, the highest cellular viability was observed at 15 µg/mL when treated with the powdered leaf and stem AgNPs. Furthermore, at 240 µg/mL, the lowest percentage for cell viability was observed in the fresh stem AgNPs (Figure 11A). Medium-high cytotoxicity was observed with the synthesized NPs even at lower concentrations (15 µg/mL). The percentage of cellular viability for HeLa was highest at 15 µg/mL when exposed to the powdered stem AgNPs, whereas at 240 µg/mL the lowest viability was observed when exposed to the methanol stem AgNPs (Figure 11B). The percentage viability for the MCF-7 cell line was greatest at 15 µg/mL when exposed to the powdered stem AgNPs, and lowest at 240 µg/mL when treated with the methanol stem and fresh leaf AgNPs (Figure 11C). Cell viabilities were above 30% for most NPs at varying concentrations (Figure 11A–C). As the NP concentration increased, so did their toxicity for the cell lines. Statistical analysis showed that all extracts had significantly different activities across all concentrations ($p < 0.05$).

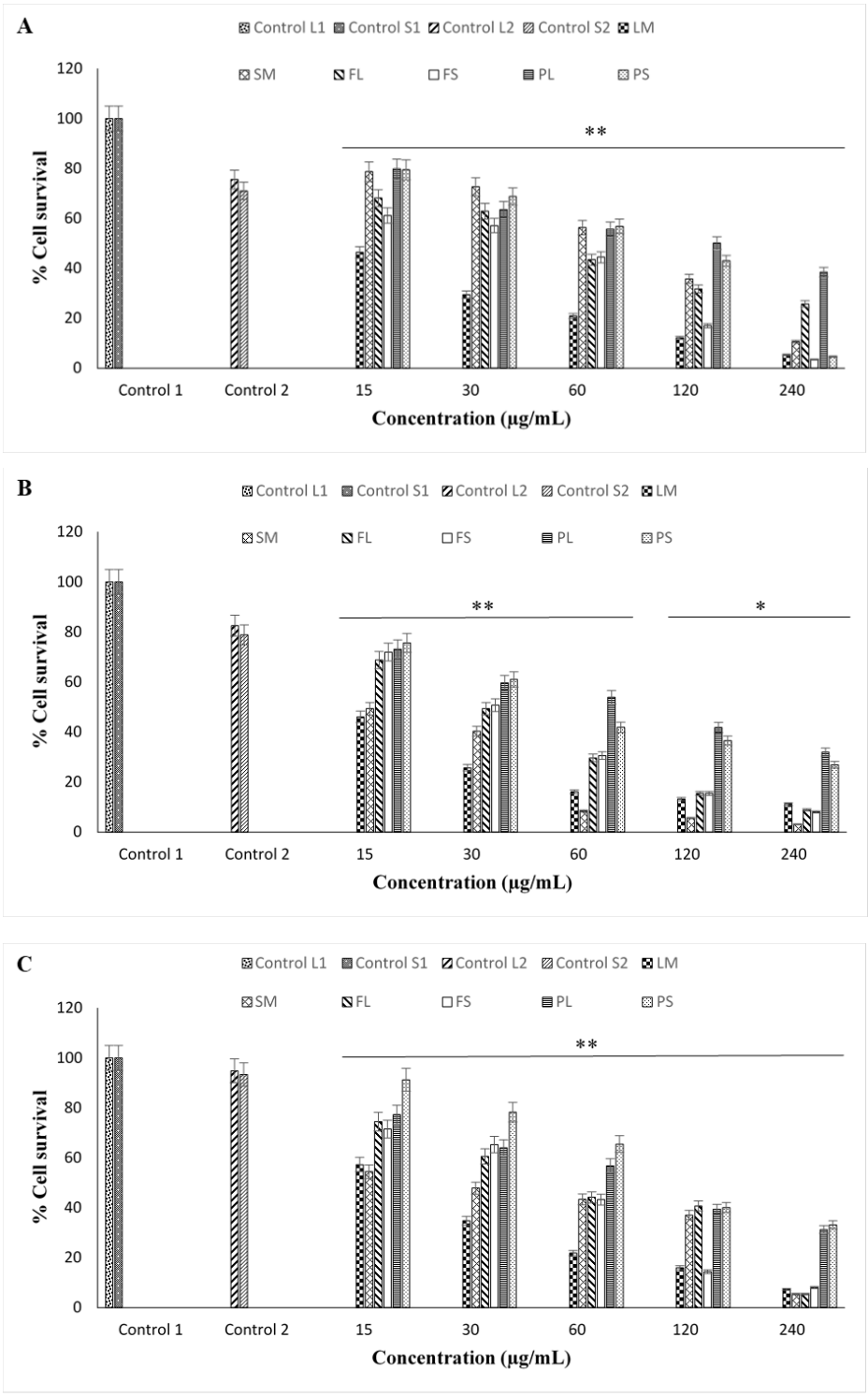

Figure 11. The in vitro cytotoxicity assessment (% cell viability) of silver nanoparticles (AgNPs) derived from the leaf and stem extracts of *B. albostellata*. (**A**) HEK293 human embryonic kidney cells; (**B**) HeLa cervical carcinoma cells; (**C**) MCF-7 breast adenocarcinoma cells. (* p <0.05 and ** p <0.001 were deemed statistically significant across the varying concentrations, ranging from 15 to 240 µg/mL). The results are expressed as means ± standard deviation (SD), with n = 3, and represented as a percentage relative to the control sample. Control Leaves 1—cells only; Control Stems 1—cells only; Control Leaves 2—DMSO control only; Control Stems 2—DMSO control; LM—Leaf methanol extract; SM—Stem methanol extract; FL—Fresh leaf material; FS—Fresh stem material; PL—Ground leaf powder; PS—Ground stem powder.

The IC_{50} values of the synthesized AgNPs in the three mammalian cell lines are represented in Table 6. Significant cytotoxic activity was observed in the HEK293 cell line upon exposure to the methanol leaf AgNPs, with an IC_{50} value of 9.02 µg/mL. However, lower cytotoxicity was found in the stem AgNPs (61.66 µg/mL). Fresh leaf and stem AgNPs displayed moderate cytotoxicity in the HEK293 cell line (IC_{50} 47.86 and 33.04 µg/mL), while lower cytotoxic levels were observed for the powdered leaf and stem AgNPs (IC_{50} 100 and 61.24 µg/mL) (Table 5). Methanol leaf and stem AgNPs displayed the highest cytotoxicity in the HeLa cell line, with IC_{50} values of 5.87 and 12.58 µg/mL, respectively. Fresh leaf and stem AgNPs displayed moderate cytotoxicity in the HeLa cell line (IC_{50} 29.64 and 32.14 µg/mL), whereas lower cytotoxic levels were observed in the powdered leaf and stem AgNPs (IC_{50} 69.18 and 54.70 µg/mL) (Table 6).

Table 6. IC_{50} values of the cytotoxicity activity of methanol, powder and fresh leaf and stem extracts of *B. albostellata*.

Cell Lines	Extracts	Cytotoxicity (µg/mL)	
		Leaves	Stems
HEK293	Methanol	9.02	61.66
	Fresh	47.86	33.04
	Powder	100.00	61.24
HeLa	Methanol	5.87	12.58
	Fresh	29.64	32.14
	Powder	69.18	54.70
MCF-7	Methanol	16.11	27.23
	Fresh	47.86	41.30
	Powder	74.13	100.00

Data are presented as mean. $n = 3$.

Significant cytotoxic levels (IC_{50} 16.11 and 27.23 µg/mL) were observed for the MCF-7 cell line upon exposure to the methanolic leaf and stem AgNPs. Moderate cytotoxic levels were observed in the fresh leaf and stem AgNPs (47.86 and 41.30 µg/mL), and lower levels in the powdered leaf and stem AgNPs (74.13 and 100 µg/mL) (Table 6). Chen and Schluesener [125] have proposed that AgNPs interact with the thiol groups of the inner membrane of the mitochondria, inhibiting the antioxidant defense mechanism, leading to the formation of reactive oxygen species (ROS). The accumulation of ROS results in an inflammatory response that initiates the destruction of the mitochondria, triggering the release of apoptogenic factors leading to cell death.

NPs are small in size, allowing them to easily enter and interact with cancer cells, and ultimately disturb cellular functions [126]. Additionally, Sanpui et al. [127] have proposed that AgNPs have the potential to interfere with genes associated with cell cycle progression, thus inducing DNA damage and apoptosis in cancerous cells. Furthermore, Jeyaraj et al. [128] have suggested that there are different mechanisms for the cytotoxicity of AgNPs, which include the induction of ROS, apoptosis, and Ag ion release. Hussain et al. [129] have observed an increase in the generation of ROS as NP concentrations are increased. Therefore, it can be expected that any cytotoxic effects induced in the cancer cells may be due to the active bound compounds capping the AgNPs.

Biosynthetic methods using plant extracts act as reducing and capping agents [14,19–21]. Using various microscopic techniques, AgNPS of similar shapes and sizes found in *B. albostellata* were noted in other species of *Barleria* [15,80]. The biosynthesized AgNPs from the leaves and stem extracts exhibited antibacterial activity against both Gram-positive and Gram-negative bacteria; this was also noted in several species of *Barleria* [80,86,90]. The precise mechanism for synthesizing NPs using plant extracts is unclear. It has been shown that biomolecules such as alkaloids, phenols, and flavonoids found in these extracts play an important role in reducing the metal ions and capping the biosynthesized NPs [26,27]. Synthesized AgNPs exhibited selective in vitro cytotoxicity against HEK293, HeLa, and

MCF-7 cell lines. The size of the NPs allow them to easily enter and interact with cancer cells, ultimately enabling them to disturb cellular functions [66]. AgNPs possess the capability to disrupt genes linked to the advancement of the cell cycle, consequently initiating DNA damage and apoptosis in cancerous cells. The cytotoxic consequences observed in the cancer cells might be attributed to the bioactive molecules capping the AgNPs [67].

4. Conclusions

A rapid, efficient, and environmentally-friendly synthesis of AgNPs was established using extracts from the leaves and stems of *B. albostellata*, offering a viable alternative to conventional chemical synthesis, particularly for medical and pharmaceutical purposes. The advantageous morphology, small dimensions, and zeta potential of the AgNPs bode well for their potential biological applications. The FTIR spectra revealed absorptions associated with various functional groups. Various phytochemical groups play an important role in the bio-reduction and stabilization of the AgNPs. The synthesized AgNPs displayed potential bacteriostatic effects against both Gram-positive and Gram-negative human pathogenic bacteria. Their wide-ranging bioactivity hints at their potential as effective agents against infections. All AgNPs exhibited cytotoxicity in vitro, with some selectivity to cancer cell lines, suggesting their promise as potential chemotherapeutic agents. Given the influence of NP surface charge on their effectiveness, it is advisable to utilize moderately stable AgNPs for further assessment. As this research signifies the inaugural exploration into the synthesis and characterization of silver nanoparticles (AgNPs) derived from *B. albostellata*, subsequent investigations should concentrate on identifying the specific biochemical components that facilitate this synthesis. To the best of our knowledge, this is the first report on the synthesis, characterization, antibacterial, and cytotoxic activities of AgNPs synthesized from the extracts of *B. albostellata*. This study sets the stage for forthcoming research to delve deeper into the therapeutic potential of AgNPs derived from *B. albostellata*. While the current characterization and assessment represent a crucial initial phase, additional experiments and tests are necessary to enhance and broaden our understanding of the impacts of these nanoparticles in antibacterial and anticancer applications. The findings of this study could significantly contribute to progressing the development of innovative phytochemical-based green compounds for potential application in the healthcare sector.

Author Contributions: Conceptualization and methodology, S.G.; investigation and data curation, S.G., Y.N., M.S., A.N.D. and J.L.; validation, S.G., Y.N., Y.H.D. and M.S.; writing—original draft preparation, S.G., Y.N. and M.S.; writing—review and editing, Y.H.D. and N.M.-D.; supervision, Y.N., Y.H.D. and M.S. All authors have read and agreed to the published version of the manuscript.

Funding: This research was funded by the National Research Foundation (grant number: 118897) and Researchers Supporting Project (grant number: RSP-2024R375), King Saud University, Riyadh, Saudi Arabia.

Institutional Review Board Statement: Not applicable.

Informed Consent Statement: Not applicable.

Data Availability Statement: The original contributions presented in the study are included in the article, further inquiries can be directed to the corresponding author.

Acknowledgments: Authors extend their appreciation to the National Research Foundation (Grant No. 118897), South Africa and the staff at the Microscopy and Microanalysis Unit at the University of KwaZulu–Natal for their assistance with the microscopy components of the research. The authors gratefully acknowledge Researchers Supporting Project number (RSP-2024R375), King Saud University, Riyadh, Saudi Arabia.

Conflicts of Interest: The authors declare no conflicts of interest.

References

1. Khatoon, N.; Mazumder, J.A.; Sardar, M. Biotechnological applications of green synthesized silver nanoparticles. *J. Nanosci. Curr. Res.* **2017**, *2*, 2572–2813. [CrossRef]
2. Pirtarighat, S.; Ghannadnia, M.; Baghshahi, S. Green synthesis of silver nanoparticles using the plant extract of *Salvia spinosa* grown in vitro and their antibacterial activity assessment. *J. Nanostruct. Chem.* **2019**, *9*, 1–9. [CrossRef]
3. Jadoun, S.; Arif, R.; Jangid, N.K.; Meena, R.K. Green synthesis of nanoparticles using plant extracts: A review. *Environ. Chem. Lett.* **2020**, *19*, 355–374. [CrossRef]
4. Ahmed, S.; Ahmad, M.; Swami, B.L.; Ikram, S. A review on plants extract mediated synthesis of silver nanoparticles for antimicrobial applications: A green expertise. *J. Adv. Res.* **2016**, *7*, 17–28. [CrossRef]
5. Viswanathan, S.; Palaniyandi, T.; Shanmugam, R.; Karunakaran, S.; Pandi, M.; Wahab, M.R.A.; Baskar, G.; Rajendran, B.K.; Sivaji, A.; Moovendhan, M. Synthesis, characterization, cytotoxicity, and antimicrobial studies of green synthesized silver nanoparticles using red seaweed *Champia parvula*. *Biomass Convers. Biorefin.* **2024**, *14*, 7387–7400. [CrossRef]
6. Iravani, S. Green synthesis of metal nanoparticles using plants. *Green Chem.* **2011**, *13*, 2638–2650. [CrossRef]
7. Vanaja, M.; Annadurai, G. *Coleus aromaticus* leaf extract mediated synthesis of silver nanoparticles and its bactericidal activity. *Appl. Nanosci.* **2012**, *9*, 217–223. [CrossRef]
8. Singh, T.; Singh, A.; Wang, W.; Yadav, D.; Kumar, A.; Singh, P.K. Biosynthesized nanoparticles and its implications in agriculture. In *Biological Synthesis of Nanoparticles and Their Applications*; CRC Press: Boca Raton, FL, USA, 2019; pp. 257–274.
9. Pal, G.; Rai, P.; Pandey, A. Green synthesis of nanoparticles: A greener approach for a cleaner future. In *Green Synthesis, Characterization and Applications of Nanoparticles SBT-GS Micro and Nano Technologies*; Shukla, A.K., Ed.; Elsevier: Amsterdam, The Netherlands, 2019; pp. 1–26.
10. Ghosh, S.; Chacko, M.J.; Harke, A.N.; Gurav, S.P.; Joshi, K.A.; Dhepe, A.; Kulkarni, A.S.; Shinde, V.S.; Parihar, V.S.; Asok, A.; et al. *Barleria prionitis* leaf mediated synthesis of silver and gold nanocatalysts. *J. Nanomed. Nanotechnol.* **2016**, *7*, 394. [CrossRef]
11. Thuesombat, P.; Hannongbua, S.; Akasit, S.; Chadchawan, S. Effect of silver nanoparticles on rice (*Oryza sativa* L. cv. KDML 105) seed germination and seedling growth. *Ecotoxicol. Environ. Saf.* **2014**, *104*, 302–309. [CrossRef]
12. Singh, J.; Dutta, T.; Kim, K.H.; Rawat, M.; Samddar, P.; Kumar, P. Green synthesis of metals and their oxide nanoparticles: Applications for environmental remediation. *J. Nanobiotechnol.* **2018**, *16*, 84. [CrossRef]
13. Ahmed, S.; Chaudhry, S.A.; Ikram, S. A review on biogenic synthesis of ZnO nanoparticles using plant extracts and microbes: A prospect towards green chemistry. *J. Photochem. Photobiol. B Biol.* **2017**, *166*, 272–284. [CrossRef] [PubMed]
14. Gardea-Torresdey, J.L.; Parsons, J.G.; Gomez, E.; Peralta-Videa, J.; Troiani, H.E.; Santiago, P.; Jose Yacaman, M. Formation and growth of Au nanoparticles inside live Alfalfa plants. *Nano Lett.* **2002**, *2*, 397–401. [CrossRef]
15. Shankar, S.S.; Ahmad, A.; Sastry, M. Geranium leaf assisted biosynthesis of silver nanoparticles. *Biotechnol. Prog.* **2003**, *19*, 1627–1631. [CrossRef] [PubMed]
16. Chandran, S.P.; Chaudhary, M.; Pasricha, R.; Ahmad, A.; Sastry, M. Synthesis of gold nanotriangles and silver nanoparticles using Aloe vera plant extract. *Biotechnol. Prog.* **2006**, *22*, 577–583. [CrossRef]
17. Smitha, S.L.; Philip, D.; Gopchand, K.G. Green synthesis of gold nanoparticles using *Cinnamomum zeylanicum* leaf broth. *Spectronochim. Acta Part A Mol. Biomol. Spectrosc.* **2009**, *74*, 735–739. [CrossRef]
18. Zhu, K.; Ju, Y.; Xu, J.; Yang, Z.; Gao, S.; Hou, Y. Magnetic nanomaterials: Chemical design, synthesis, and potential applications. *Acc. Chem. Res.* **2018**, *51*, 404–413. [CrossRef] [PubMed]
19. Krishnaraj, C.; Jagan, E.G.; Rajasekar, S.; Selvakumar, P.; Kalaichelvan, P.T.; Mohan, N.J.C.S.B.B. Synthesis of silver nanoparticles using *Acalypha indica* leaf extracts and its antibacterial activity against water borne pathogens. *Colloids Surf. B Biointerfaces* **2010**, *76*, 50–56. [CrossRef]
20. El-Seedi, H.R.; El-Shabasy, R.M.; Khalifa, S.A.; Saeed, A.; Shah, A.; Shah, R.; Iftikhar, F.J.; Abdel-Daim, M.M.; Omri, A.; Hajrahand, N.H.; et al. Metal nanoparticles fabricated by green chemistry using natural extracts: Biosynthesis, mechanisms, and applications. *RSC. Adv.* **2019**, *9*, 24539–24559. [CrossRef]
21. MR, K.P.; Iyer, P.R. Antiproliferative effects on tumor cells of the synthesized gold nanoparticles against Hep2 liver cancer cell line. *Egypt Liver J.* **2020**, *10*, 15.
22. Lee, H.J.; Lee, G.; Jang, N.R.; Yun, J.H.; Song, J.Y.; Kim, B.S. Biological synthesis of copper nanoparticles using plant extract. *Nanotechnology* **2011**, *1*, 371–374.
23. Kim, J.S.; Kuk, E.; Yu, K.N.; Kim, J.H.; Park, S.J.; Lee, H.J.; Cho, M.H. Antimicrobial effects of silver nanoparticles. *Nano Med. NBM* **2007**, *3*, 95–101. [CrossRef] [PubMed]
24. Rai, M.; Yadav, A.; Gade, A. Silver nanoparticles as a new generation of antimicrobials. *Biotechnol. Adv.* **2009**, *27*, 76–83. [CrossRef]
25. Azócar, M.I.; Alarcón, R.; Castillo, A.; Blamey, J.M.; Walter, M.; Paez, M. Capping of silver nanoparticles by anti-inflammatory ligands: Antibacterial activity and superoxide anion generation. *J. Photochem. Photobiol. B Biol.* **2019**, *193*, 100–108. [CrossRef]
26. Lee, K.S.; El-Sayed, M.A. Gold and silver nanoparticles in sensing and imaging: Sensitivity and plasmon response to size, shape, and metal composition. *J. Phys. Chem. B* **2006**, *110*, 19220–19225. [CrossRef] [PubMed]
27. WHO. Cancer Key Facts. 2021. Available online: https://www.who.int/news-room/fact-sheets/detail/cancer (accessed on 3 September 2021).
28. Jamison, D.T.; Feachem, R.G.; Makgoba, M.W. *Disease and Mortality in Sub-Saharan Africa*; World Bank: Washington, DC, USA, 2006.

29. Zhang, Y.; Hong, H.; Cai, W. Tumor-targeted drug delivery with aptamers. *Curr. Med. Chem.* **2011**, *18*, 4185–4194. [CrossRef]
30. Nikolaou, M.; Pavlopoulou, A.; Georgakilas, A.G.; Kyrodimos, E. The challenge of drug resistance in cancer treatment: A current overview. *Clin. Exp. Metastas.* **2018**, *35*, 309–318. [CrossRef]
31. Anselmo, A.C.; Mitragotri, S. An overview of clinical and commercial impact of drug delivery systems. *J. Control Release* **2014**, *190*, 15–28. [CrossRef] [PubMed]
32. Wang, S.; Li, Y.; Ju, D. Application of nanomaterials for cancer diagnosis and therapy. In *Green Synthesis of Nanoparticles: Applications and Prospects*; Springer: Singapore, 2020; pp. 121–140.
33. Mandal, S.M.; Roy, A.; Mahata, D.; Migliolo, L.; Nolasco, D.O.; Franco, O.L. Functional and structural insights on self-assembled nanofiber-based novel antibacterial ointment from antimicrobial peptides, bacitracin and gramicidin S. *J. Antibiot.* **2014**, *67*, 771–775. [CrossRef] [PubMed]
34. Jha, A.K.; Prasad, K.; Prasad, K.; Kulkarni, A.R. Plant system: Nature's nanofactory. *Colloids Surf. B Biointerfaces* **2009**, *73*, 219–223. [CrossRef]
35. Chandirika, J.U.; Annadurai, G. Biosynthesis and characterization of silver nanoparticles using leaf extract *Abutilon indicum*. *Glob. J. Biotechnol. Biochem.* **2018**, *13*, 7–11.
36. Vasanth, K.; Ilango, K.; Mohan-Kumar, R.; Agrawal, A.; Dubey, G.P. Anticancer activity of *Moringa oleifera* mediated silver nanoparticles on human cervical carcinoma cells by apoptosis induction. *Colloids Surf. B Biointerfaces* **2014**, *117*, 354–359. [CrossRef] [PubMed]
37. Hembram, K.C.; Kumar, R.; Kandha, L.; Parhi, P.K.; Kundu, C.N.; Bindhani, B.K. Therapeutic prospective of plant-induced silver nanoparticles: Application as antimicrobial and anticancer agent. *Artif. Cells Nanomed. Biotechnol.* **2018**, *46*, S38–S51. [CrossRef]
38. Larue, C.; Castillo-Michel, H.; Sobanska, S.; Cécillon, L.; Bureau, S.; Barthès, V.; Ouerdane, L.; Carrière, M.; Sarret, G. Foliar exposure of the crop *Lactuca sativa* to silver nanoparticles: Evidence for internalization and changes in Ag speciation. *J. Hazard. Mater.* **2014**, *264*, 98–106. [CrossRef]
39. Mussin, J.; Robles-Botero, V.; Casañas-Pimentel, R.; Rojas, F.; Angiolella, L.; Martín-Martínez, S.; Giusiano, G. Antimicrobial an cytotoxic activity of green synthesis silver nanoparticles targeting skin and soft tissue infectious agents. *Sci Rep.* **2021**, *11*, 14566. [CrossRef] [PubMed]
40. Sharma, S.; Kumar, S.; Bulchandini, B.; Taneja, S.; Banyal, S. Green synthesis of silver nanoparticles and their antimicrobial activity against Gram positive and Gram negative bacteria. *Int. J. Biotechnol. Mol. Biol. Res.* **2013**, *4*, 711–714.
41. Begum, M.Y.; Sirisha, C.H.; Reddy, G.P. Nanoparticulate drug delivery system-an overview. *Int. J. Biotechnol. Mol. Biol. Res.* **2017**, *1*, 15–25.
42. Chinnasamy, C.; Tamilselvan, P.; Karthik, V.; Karthik, B. Optimization and characterization studies on green synthesis of silver nanoparticles using response surface methodology. *J. Adv. Res. Nat. Appl. Sci.* **2017**, *11*, 214–221.
43. Maddila, S.; Hemalatha, K.P.J. Phytochemical screening and in vitro antimicrobial properties of crude leaf extracts of Wrightia tinctoria R.Br. *Int. J. Curr. Microbiol. Appl. Sci.* **2017**, *6*, 707–720. [CrossRef]
44. Nguyen, N.P.U.; Dang, N.T.; Doan, L.; Nguyen, T.T.H. Synthesis of Silver Nanoparticles: From Conventional to 'Modern' Methods—A Review. *Processes* **2023**, *11*, 2617. [CrossRef]
45. Vishwanath, R.; Negi, B. Conventional and green methods of synthesis of silver nanoparticles and their antimicrobial properties. *Curr. Res. Green Sustain. Chem.* **2021**, *4*, 100205. [CrossRef]
46. Salam, H.A.; Rajiv, P.; Kamaraj, M.; Jagadeeswaran, P.; Gunalan, S.; Sivaraj, R. Plants: Green route for nanoparticle synthesis. *Int. Res. J. Biol. Sci.* **2012**, *1*, 85–90.
47. Froneman, W.; Le Roux, L.N. *Barleria albostellata*. 2007. Available online: http://pza.sanbi.org/barleria-albostellata (accessed on 2 February 2019).
48. Amoo, S.O.; Finnie, J.F.; Van Staden, J. In vitro pharmacological evaluation of three *Barleria* species. *J. Ethnopharmacol.* **2009**, *121*, 274–277. [CrossRef] [PubMed]
49. Yosook, C.; Panpisutchai, Y.; Chaichana, S.; Santisuk, T.; Reutrakul, V. Evaluation of anti-HSV-2 activities of *Barleria lupulina* and *Clinacanthus nutans*. *J. Ethnopharmacol.* **1999**, *67*, 179–187. [CrossRef] [PubMed]
50. Wang, B.U.; Wu, M.; Perchellet, E.M.; Mcilvain, C.J.; Sperfslage, B.J.; Huang, X.; Tamura, M.; Stephany, H.A.; Hua, D.H.; Perchellet, J.P. Asynthetic triptycene bisquinone which blocks nucleoside transport and induces DNA fragmentation, retains its cytotoxic efficacy in daunorubicin-resistant HL-60 cell lines. *Int. J. Oncol.* **2001**, *19*, 1169–1178. [PubMed]
51. Jassim, S.A.A.; Naji, A.M. Novel antiviral agents: A medicinal plant perspective. *J. Appl. Microbiol.* **2003**, *95*, 412–427. [CrossRef] [PubMed]
52. Suba, V.; Murugesan, T.; Arunachalam, G.; Mandal, S.C.; Saha, B.P. Anti-diabetic potential of *Barleria lupulina* extract in rats. *Phytomedicine* **2004**, *11*, 202–205. [CrossRef]
53. Suba, V.; Murugesan, T.; Kumaravelrajan, R.; Mandal, S.C.; Saha, B.P. Antiinflammatory, analgesic and antiperoxidative efficacy of *Barleria lupulina* Lindl. extract. *Phytother. Res.* **2005**, *19*, 695–699. [CrossRef]
54. Chomnawang, M.T.; Surassmo, S.; Nukoolkarn, V.S.; Gritsanapan, W. Antimicrobial effects of Thai medicinal plants against acne-inducing bacteria. *J. Ethnopharmacol.* **2005**, *101*, 330–333. [CrossRef]
55. Shukla, S.; Gunjegaokar, S.M. Pharmacognostical and pharmacological profiling of *Barleria prionitis* Linn. *J. Biol. Sci. Med.* **2018**, *4*, 41–50.

56. Gangaram, S.; Naidoo, Y.; Dewir, Y.H.; Singh, M.; Lin, J.; Murthy, H.N. Phytochemical Composition and Antibacterial Activity of *Barleria albostellata* C.B. Clarke Leaf and Stem Extracts. *Plants* **2023**, *12*, 2396. [CrossRef]
57. Gangaram, S.; Naidoo, Y.; Dewir, Y.H.; Singh, M.; Daniels, A.N.; Magyar-Tábori, K.; Mendler-Drienyovszki, N. Antiox-idant and Cytotoxic Activities of Leaf and Stem Extracts of *Barleria albostellata* CB Clarke. *Horticulturae* **2023**, *9*, 1226. [CrossRef]
58. Akula, R.; Ravishankar, G.A. Influence of abiotic stress signals on secondary metabolites in plants. *Plant Signal. Behav.* **2011**, *6*, 1720–1731. [CrossRef]
59. Kannan, R.R.R.; Stirk, W.A.; Van Staden, J. Synthesis of silver nanoparticles using the seaweed *Codium capitatum* P.C *Silva* (Chlorophyceae). *S. Afr. J. Bot.* **2013**, *86*, 1–4. [CrossRef]
60. Govindarajan, M.; Benelli, G. Facile biosynthesis of silver nanoparticles using *Barleria cristata*: Mosquitocidal potential and biotoxicity on three non-target aquatic organisms. *Parasitol. Res.* **2016**, *115*, 925–935. [CrossRef]
61. Cittrarasu, V.; Balasubramanian, B.; Kaliannan, D.; Park, S.; Maluventhan, V.; Kaul, T.; Liu, W.C.; Arumugam, M. Biological mediated Ag nanoparticles from *Barleria longiflora* for antimicrobial activity and photocatalytic degradation using methylene blue. *Artif. Cells Nanomed. Biotechnol.* **2019**, *47*, 2424–2430. [CrossRef]
62. Premasudha, P.; Venkataramana, M.; Abirami, M.; Vanathi, P.; Krishna, K.; Rajendran, R. Biological synthesis and characterization of silver nanoparticles using *Eclipta alba* leaf extract and evaluation of its cytotoxic and antimicrobial potential. *Bull. Mater. Sci.* **2015**, *38*, 965–973. [CrossRef]
63. Gunasekaran, K.; Nirmala, M.; Raja, K.; Saravanakumar, A. Characterization and application of biosynthesized silver nanoparticles from *Melia dubia* leaves. *Ind. J. Geo-Mar. Sci.* **2017**, *46*, 1715–1720.
64. Moodley, J.S.; Krishna, S.B.N.; Pillay, K.; Govender, P. Green synthesis of silver nanoparticles from *Moringa oleifera* leaf extracts and its antimicrobial potential. *Adv. Nat. Sci. Nanosci. Nanotechnol.* **2018**, *9*, 015011. [CrossRef]
65. Daniels, A.N.; Singh, M. Sterically stabilized siRNA: Gold nanocomplexes enhance c-MYC silencing in a breast cancer cell model. *Nanomedicine* **2019**, *14*, 1387–1401. [CrossRef]
66. Mosman, T. Rapid colourimetric assay for cellular growth and survival: Application to proliferation and cytotoxicity assays. *J. Immunol. Meth.* **1983**, *65*, 55–63. [CrossRef]
67. Vinken, M.; Blaauboer, B.J. In vitro testing of basal cytotoxicity: Establishment of an adverse outcome pathway from chemical insult to cell death. *Toxicol. In Vitro* **2017**, *39*, 104–110. [CrossRef]
68. Mulvaney, P. Surface plasmon spectroscopy of nanosized metal particles. *Langmuir* **1996**, *12*, 788–800. [CrossRef]
69. Jensen, T.R.; Schatz, G.C.; Van Duyne, R.P. Nanosphere lithography: Surface plasmon resonance spectrum of a periodic array of silver nanoparticles by ultraviolet−visible extinction spectroscopy and electrodynamic modeling. *J. Phys. Chem.* **1999**, *103*, 2394–2401. [CrossRef]
70. Heemasagar, D.; Jeeva, K.; Sureshkumar, M. Enhanced anti-microbial activity of honey with green synthesized AgNps by using *Tabernaemontana coronaria* (JACQ.) wild flower extract. *Am. J. PharmTech Res.* **2014**, *4*, 1–12.
71. Jiang, X.; Chen, W.; Chen, C.; Xiong, S.; Yu, A. Role of temperature in the growth of silver nanoparticles through a synergetic reduction approach. *Nanoscale Res. Lett.* **2011**, *6*, 32. [CrossRef]
72. Bogireddy, N.K.R.; Kumar, H.A.K.; Mandal, B.K. Biofabricated silver nanoparticles as green catalyst in the degradation of different textile dyes. *J. Environ. Chem. Eng.* **2016**, *4*, 56–64. [CrossRef]
73. De Aragaõ, A.P.; De Oliveira, T.M.; Quelemes, P.V.; Perfeito, M.L.G.; Araujo, M.C.; Santiago, J.D.A.S.; Cardoso, V.S.; Quaresma, P.; De Souza De Almeida Leite, J.R.; Da Silva, D.A. Greensynthesis of silver nanoparticles using the seaweed *Gracilariabirdiae* and their antibacterial activity. *Arab. J. Chem.* **2019**, *12*, 4182–4188. [CrossRef]
74. MubarakAli, D.; Thajuddin, N.; Jeganathan, K.; Gunasekaran, M. Plant extract mediated synthesis of silver and gold nanoparticles and its antibacterial activity against clinically isolated pathogens. *Colloids Surf. B Biointerfaces* **2011**, *85*, 360–365. [CrossRef]
75. Gomathi, M.; Rajkumar, P.V.; Prakasam, A. Study of dislocation density (defects such as Ag vacancies and interstitials) of silver nanoparticles, green-synthesized using *Barleria cristata* leaf extract and the impact of defects on the antibacterial activity. *Results Phys.* **2018**, *10*, 858–864. [CrossRef]
76. Bello, B.A.; Khan, S.A.; Khan, J.A.; Syed, F.Q.; Mirza, M.B.; Shah, L.; Khan, S.B. Anticancer, antibacterial and pollutant degradation potential of silver nanoparticles from *Hyphaene thebaica*. *Biochem. Biophys. Res. Commun.* **2017**, *490*, 889–894. [CrossRef]
77. Ahluwalia, V.; Kumar, J.; Sisodia, R.; Shakil, N.A.; Walia, S. Green synthesis of silver nanoparticles by *Trichoderma harzianum* and their bio-efficacy evaluation against *Staphylococcus aureus* and *Klebsiella pneumonia*. *Ind. Crop. Prod.* **2014**, *55*, 202–206. [CrossRef]
78. Muthukrishnan, S.; Bhakya, S.; Kumar, T.S.; Rao, M.V. Biosynthesis, characterization and antibacterial effect of plant-mediated silver nanoparticles using *Ceropegia thwaitesii*—An endemic species. *Ind. Crop. Prod.* **2015**, *63*, 119–124. [CrossRef]
79. Kumar, V.; Yadav, S.C.; Yadav, S.K. *Syzygium cumini* leaf and seed extract mediated biosynthesis of silver nanoparticles and their characterization. *J. Chem. Technol. Biotechnol.* **2010**, *85*, 1301–1309. [CrossRef]
80. Patel, N. Biosynthesis and Antibacterial Activity of Silver and Gold Nanoparticles from the Leaf and Callus Extracts of *Amaranthus dubius*, *Gunnera perpensa*, *Ceratotheca triloba* and *Catharanthus roseus*. Ph.D. Thesis, Durban University of Technology, Durban, South Africa, 2013.
81. Shao, F.; Yang, A.; Yu, D.M.; Wang, J.; Gong, X.; Tian, H.X. Bio-synthesis of *Barleria gibsoni* leaf extract mediated zinc oxide nanoparticles and their formulation gel for wound therapy in nursing care of infants and children. *J. Photochem. Photobiol. B* **2018**, *189*, 267–273. [CrossRef]

82. Nayak, D.; Pradhan, S.; Ashe, S.; Rauta, P.R.; Nayak, B. Biologically synthesised silver nanoparticles from three diverse family of plant extracts and their anticancer activity against epidermoid A431 carcinoma. *J. Colloid Interface Sci.* **2015**, *457*, 329–338. [CrossRef]
83. Verma, A.; Mehata, M.S. Controllable synthesis of silver nanoparticles using *Neem* leaves and their antimicrobial activity. *J. Radiat. Res. Appl. Sci.* **2016**, *9*, 109–115. [CrossRef]
84. Mallikarjuna, K.; Narasimha, G.; Dillip, G.R.; Praveen, B.; Shreedhar, B.; Shree Lakshmi, C.; Reddy, B.V.S.; Deva Prasad Raju, B. Green synthesis of silver nanoparticles using *Ocimim* leaf extract and their characterization. *Digest J. Nanomater. Biostruct.* **2011**, *6*, 181–186.
85. Restrepo, C.V.; Villa, C.C. Synthesis of silver nanoparticles, influence of capping agents, and dependence on size and shape: A review. *Environ. Nanotechnol. Monit. Manag.* **2021**, *15*, 100428. [CrossRef]
86. Mittal, A.K.; Chisti, Y.; Banerjee, U.C. Synthesis of metallic nanoparticles using plant extracts. *Biotechnol. Adv.* **2013**, *31*, 346–356. [CrossRef]
87. Akinyelu, J.; Singh, M. Folate-tagged chitosan functionalized gold nanoparticles for enhanced delivery of 5-fluorouracil to cancer cells. *Appl. Nanosci.* **2019**, *9*, 7–17. [CrossRef]
88. Oladimeji, O.; Akinyelu, J.; Daniels, A.; Singh, M. Modified Gold Nanoparticles for efficient delivery of Betulinic Acid to cancer cell mitochondria. *Int. J. Mol. Sci.* **2021**, *22*, 5072. [CrossRef]
89. Honary, S.; Zahir, F. Effect of zeta potential on the properties of nano-drug delivery systems—A review (Part 1). *Trop. J. Pharm. Res.* **2013**, *12*, 255–264.
90. Joseph, E.; Singhvi, G. Multifunctional nanocrystals for cancer therapy: A potential nanocarrier. *Nanomed. Drug Deliv. Ther.* **2019**, 91–116.
91. Griffiths, D.; Bernt, W.; Hole, P.; Smith, J.; Malloy, A.; Carr, B. Zeta potential measurement of nanoparticles by nanoparticle tracking analysis (NTA). *NSTI-Nanotech* **2011**, *1*, 4–7.
92. Hunter, R.J. *Zeta Potential in Colloid Science: Principles and Applications*; Academic Press: Cambridge, MA, USA, 2013.
93. Freitas, C.; Müller, R.H. Effect of light and temperature on zeta potential and physical stability in solid lipid nanoparticle (SLN™) dispersions. *Int. J. Pharm.* **1998**, *168*, 221–229. [CrossRef]
94. Shah, R.; Eldridge, D.; Palombo, E.; Harding, I. Optimisation and stability assessment of solid lipid nanoparticles using particle size and zeta potential. *J. Phys. Sci.* **2014**, *25*, 59–75.
95. Chorom, M.; Rengasamy, P. Dispersion and zeta potential of pure clays as related to net particle charge under varying pH, electrolyte concentration and cation type. *Eur. J. Soil Sci.* **1995**, *46*, 657–665. [CrossRef]
96. Dubey, S.P.; Lahtinen, M.; Sillanpää, M. Tansy fruit mediated greener synthesis of silver and gold nanoparticles. *Process Biochem.* **2010**, *45*, 1065–1071. [CrossRef]
97. Basnet, P.; Amarasiriwardena, D.; Wu, F.; Fu, Z.; Zhang, T. Investigation of tissue level distribution of functional groups and associated trace metals in rice seeds (*Oryza sativa* L.) using FTIR and LA-ICP-MS. *Microchem. J.* **2016**, *127*, 152–159. [CrossRef]
98. Shanmugam, V.; Selvakumar, S.; Yeh, C.S. Near-infrared light-responsive nanomaterials in cancer therapeutics. *Chem. Soc. Rev.* **2014**, *43*, 6254–6287. [CrossRef]
99. Marimuthu, S.; Rahuman, A.A.; Rajakumar, G.; Santhoshkumar, T.; Kirthi, A.V.; Jayaseelan, C.; Bagavan, A.; Zahir, A.A.; Elango, G.; Kamaraj, C. Evaluation of green synthesized silver nanoparticles against parasites. *Parasit. Res.* **2011**, *108*, 1541–1549. [CrossRef] [PubMed]
100. Chand, K.; Cao, D.; Fouad, D.E.; Shah, A.H.; Dayo, A.Q.; Zhu, K.; Lakhan, M.N.; Mehdi, G.; Dong, S. Green synthesis, characterization and photocatalytic application of silver nanoparticles synthesized by various plant extracts. *Arab. J. Chem.* **2020**, *13*, 8248–8261. [CrossRef]
101. Heneczkowski, M.; Kopacz, M.; Nowak, D.; Kuzniar, A. Infrared spectrum analysis of some flavonoids. *Acta Pol. Pharm.* **2001**, *58*, 415–420.
102. Firdhouse, M.J.; Lalitha, P. Phyto-assisted synthesis and characterization of silver nanoparticles from *Amaranthus dubius*. *Int. J. Appl. Biol. Pharm. Technol.* **2012**, *3*, 96–101.
103. Sivakumar, J.; Premkumar, C.; Santhanam, P.; Saraswathi, N. Biosynthesis of silver nanoparticles using *Calotropis gigantean* leaf. *Afr. J. Basic Appl. Sci.* **2011**, *3*, 265–270.
104. Devaraj, P.; Kumari, P.; Aarti, C.; Renganathan, A. Synthesis and characterization of silver nanoparticles using cannonball leaves and their cytotoxic activity against MCF-7 cell line. *J. Nanotechnol.* **2013**, *2013*, 598328. [CrossRef]
105. Shahverdi, A.R.; Fakhimi, A.; Shahverdi, H.R.; Minaian, S. Synthesis and effect of silver nanoparticles on the antibacterial activity of different antibiotics against *Staphylococcus aureus* and *Escherichia coli*. Nanomed. *Nanotechnol. Biol. Med.* **2007**, *3*, 168. [CrossRef]
106. Tamayo, L.A.; Zapata, P.A.; Vejar, N.D.; Azocar, M.I.; Gulppi, M.A.; Zhou, X.; Thompson, G.E.; Rabagliati, F.M.; Paez, M.A. Release of silver and copper nanoparticles from polyethylene nanocomposites and their penetration into *Listeria* monocytogenes. *Mater. Sci. Eng. Mater.* **2014**, *40*, 24–31. [CrossRef]
107. Wu, D.; Fan, W.; Kishen, A.; Gutmann, J.L.; Fan, B. Evaluation of the antibacterial efficacy of silver nanoparticles against *Enterococcus faecalis* biofilm. *J. Endod.* **2014**, *40*, 285–290. [CrossRef]
108. Guzman, M.; Dille, J.; Godet, S. Synthesis and antibacterial activity of silver nanoparticles against gram-positive and gram-negative bacteria. *Nanomed. Nanotechnol. Biol. Med.* **2012**, *8*, 37–45. [CrossRef]

109. Sun, Q.; Cai, X.; Li, J.; Zheng, M.; Chen, Z.; Yu, C.P. Green synthesis of silver nanoparticles using tea leaf extract and evaluation of their stability and antibacterial activity. *Colloids Surf. A Physicochem. Eng. Asp.* **2014**, *444*, 226–231. [CrossRef]
110. Mohammadi, G.; Valizadeh, H.; Barzegar-Jalali, M.; Lotfipour, F.; Adibkia, K.; Milani, M.; Azhdarzadeh, M.; Kiafar, F.; Nokhodchi, A. Development of azithromycin–PLGA nanoparticles: Physicochemical characterization and antibacterial effect against Salmonella typhi. *Colloids Surf. B Biointerfaces* **2010**, *80*, 34–39. [CrossRef]
111. Seil, J.T.; Webster, T.J. Antimicrobial applications of nanotechnology: Methods and literature. *Int. J. Nanomed.* **2012**, *7*, 2767–2781.
112. Kvítek, L.; Panáček, A.; Soukupova, J.; Kolář, M.; Večeřová, R.; Prucek, R.; Holecová, M.; Zbořil, R. Effect of surfactants and polymers on stability and antibacterial activity of silver nanoparticles (NPs). *J. Phys. Chem.* **2008**, *112*, 5825–5834. [CrossRef]
113. Collins, T.L.; Markus, E.A.; Hassett, D.J.; Robinson, J.B. The effect of a cationic porphyrin on *Pseudomonas aeruginosa* biofilms. *Curr. Microb.* **2010**, *61*, 411–416. [CrossRef] [PubMed]
114. Hajipour, M.J.; Fromm, K.M.; Ashkarran, A.A.; de Aberasturi, D.J.; de Larramendi, I.R.; Rojo, T.; Serpooshan, V.; Parak, W.J.; Mahmoudi, M. Antibacterial properties of nanoparticles. *Trends Biotechnol.* **2012**, *30*, 499–511. [CrossRef] [PubMed]
115. Umashankari, J.; Inbakandan, D.; Ajithkumar, T.T.; Balasubramanian, T. Mangrove plant, *Rhizophora mucronata* (Lamk, 1804) mediated one pot green synthesis of silver nanoparticles and its antibacterial activity against aquatic pathogens. *Aqua. Biosys.* **2012**, *8*, 11. [CrossRef]
116. Lok, C.N.; Ho, C.M.; Chen, R.; He, Q.Y.; Yu, W.Y.; Sun, H.; Tam, P.K.H.; Chiu, J.F.; Che, C.M. Proteomic analysis of the mode of antibacterial action of silver nanoparticles. *J. Proteome Res.* **2006**, *5*, 916–924. [CrossRef]
117. Iavicoli, I.; Fontana, L.; Leso, V.; Bergamaschi, A. The effects of nanomaterials as endocrine disruptors. *Int. J. Mol. Sci.* **2013**, *14*, 16732–16801. [CrossRef]
118. Yun, H.; Kim, J.D.; Choi, H.C.; Lee, C.W. Antibacterial activity of CNT-Ag and GO-Ag nanocomposites against gram-negative and gram-positive bacteria. *Bull. Korean Chem. Soc.* **2013**, *34*, 3261–3264. [CrossRef]
119. Egger, S.; Lehmann, R.P.; Height, M.J.; Loessner, M.J.; Schuppler, M. Antimicrobial properties of a novel silver-silica nanocomposite material. *Appl. Environ. Microbiol.* **2009**, *75*, 2973–2976. [CrossRef] [PubMed]
120. Safavi, K. Evaluation of using nanomaterial in tissue culture media and biological activity. In Proceedings of the Second International Conference on Ecological, Environmental and Biological, Sciences, Bali, Indonesia, 13–14 October 2012.
121. Rai, M.; Kon, K.; Ingle, A.; Duran, N.; Galdiero, S.; Galdiero, M. Broad-spectrum bioactivities of silver nanoparticles: The emerging trends and future prospects. *Appl. Microbiol. Biotechnol.* **2014**, *98*, 1951–1961. [CrossRef] [PubMed]
122. van Meerloo, J.; Kaspers, G.J.; Cloos, J. Cell sensitivity assays: The MTT assay. In *Cancer Cell Culture*; Cree, I., Ed.; Humana Press: Totowa, NJ, USA, 2011; pp. 237–245.
123. Parasuraman, S. Toxicological screening. *J. Pharmacol. Pharmacother.* **2011**, *2*, 74–79.
124. Sutradhar, K.B.; Amin, M. Nanotechnology in cancer drug delivery and selective targeting. *Int. J. Nanotechnol.* **2014**, *2014*, 939378. [CrossRef]
125. Fernandes, C.; Suares, D.; Yergeri, M.C. Tumor microenvironment targeted nanotherapy. *Front. Pharmacol.* **2018**, *9*, 1230. [CrossRef]
126. Chen, X.; Schluesener, H.J. Nanosilver: A nanoproduct in medical application. *Toxicol. Lett.* **2008**, *176*, 1–12. [CrossRef]
127. Park, E.J.; Yi, J.; Kim, Y.; Choi, K.; Park, K. Silver nanoparticles induce cytotoxicity by a Trojan-horse type mechanism. *Toxicol. In Vitro* **2010**, *24*, 872–878. [CrossRef] [PubMed]
128. Sanpui, P.; Chattopadhyay, A.; Ghosh, S.S. Induction of apoptosis in cancer cells at low silver nanoparticle concentrations using chitosan nanocarrier. *ACS Appl. Mater. Interfaces* **2011**, *3*, 218–228. [CrossRef]
129. Jeyaraj, M.; Rajesh, M.; Arun, R.; MubarakAli, D.; Sathishkumar, G.; Sivanandhan, G.; Dev, G.K.; Manickavasagam, M.; Premkumar, K.; Thajuddin, N.; et al. An investigation on the cytotoxicity and caspase-mediated apoptotic effect of biologically synthesized silver nanoparticles using *Podophyllum hexandrum* on human cervical carcinoma cells. *Colloids Surf. B Biointerfaces* **2013**, *102*, 708–717. [CrossRef]